STRUCTURAL MODIFICATION OF UNIDIRECTIONALLY SOLIDIFIED ALUMINUM-SILICON EUTECTIC ALLOYS BY ANTIMONY TREATMENT

by

Ahmet İhsan Telli

B.S. in M.E., Boğaziçi University, 1982

Submitted to the Institute for Graduate Studies in Science and Engineering in partial fulfillment of the requirements for the degree of

Master of Science

in

Mechanical Engineering

Boğaziçi University

1984

STRUCTURAL MODIFICATION OF UNIDIRECTIONALLY SOLIDIFIED ALUMINUM-SILICON EUTECTIC ALLOYS BY ANTIMONY TREATMENT

APPROVED BY

Doç.Dr. Ş. Ergin KISAKÜREK (Thesis Supervisor) Ş. E. Kısakürek

Doç.Dr. Sabri ALTINTAŞ S. Altıntaş

Doç.Dr. Başar CİVELEK M. Başar Civelek

DATE OF APPROVAL

21.2.1984

ACKNOWLEDGEMENTS

I would like to express my sincere gratitude to Doç.Dr. Ş. Ergin Kısakürek for his appreciable helps and guidance during this study.

I want to acknowledge the Rabak Company for providing required aluminum material.

Especially, I would like to thank Müge Gürer for her helps in the experimental work.

I am also indepted to Osman Kurdaş and Adnan Koru for their assistance in tensile testing.

Ahmet İhsan Telli

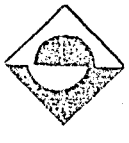

ABSTRACT

In this study, the structural modification of the unidirectionally solidified aluminum-silicon eutectic alloys with antimony treatment was investigated.

First, a general understanding of eutectic solidification was given and then modification mechanism of antimony was studied.

In the experimental work, antimony treated aluminum-silicon eutectic alloys were unidirectionally solidified and resulting microstructure was subjected to detailed investigation. Then the mechanical properties were measured with tensile testing and Vickers hardness testing.

Finally, the measured interparticle spacings have been correlated to the changes in antimony concentration, growth rate and temperature gradient.

Ö Z E T

Bu çalışmada tek yönlü katılaşma ile oluşturulan alüminyum-silikon ötektik alaşımlarında antimuan etkisi ile yapı değişikliği araştırılmıştır.

Önce, ötektik katılaşması üzerine genel bir bilgi verilmiş ve sonra antimuan modifikasyon mekanizması üzerinde çalışılmıştır.

Deneysel çalışmalarda antimuan ile etkilenmiş alüminyum-silikon alaşımları tek yönlü olarak katılaştırılmış ve ortaya çıkan iç yapı detaylı bir incelemeye tâbi tutulmuştur.

Daha sonra mekanik özellikleri çekme testi ve Vickers sertlik ölçme testi ile ölçülmüştür.

Sonuç olarak, ölçülen parçacık arası uzunlukları ile, antimuan yoğunluğu, büyüme hızı ve sıcaklık gradyanlarındaki değişmeler arasında korelasyona varılmıştır.

TABLE OF CONTENTS

LIST OF FIGURES

Page

LIST OF TABLES

LIST OF SYMBOLS

λ	Interparticle spacing
m	Temperature gradient exponent
n	Growth rate exponent
s	Cooling rate exponent
G_L	Temperature gradient
R	Growth rate
ΔS_f	Entropy of fusion
η	Number of nearest neighbours of an atom at the solid-liquid interface
u	Coordination number
L_o	Latent heat of fusion
k	Boltzmann's constant
T_E	Melting temperature
$\Delta T_D, \Delta T_C, \Delta T_K$	Compositional, curvature and kinetic undercoolings
ΔT_α, ΔT_β	Total undercoolings of α and β phase
m_L	Slope of the liquidus line
C	Liquid composition at the interface
C_E	Eutectic composition
C_o	Starting alloy composition
C_∞	Composition far away from the interface
D	Diffusion coeffient
S_α, S_β	Half width of the α and β lamellae
T	Rod spacing
$a_\alpha^L, a_\beta^L, a_\alpha^T, a_\beta^T$	Surface energy terms
$\overline{C}_o^\alpha$, $\overline{C}_o^\beta$	Average compositional differences between solid and liquid
m_α, m_β	Liquidus slopes of α and β phases
M	Tabulated function of the volume fraction
P	Tabulated function of S_α/S_β
N_L	Number of particle interceptions
F	Applied load
L	Average value of the diagonals of indentation

I. INTRODUCTION

One of the eutectics which has particular commercial importance is that between aluminum and silicon. These alloys have a relatively low density, low thermal expansion, high thermal conductivity and good mechanical properties. Aluminum alloys containing about 7 percent silicon comprise an important family of high strength structural castings. Alloys in the neighbourhood of 12 percent silicon (approximately eutectic composition) are widely used in die-casting and for applications requiring wear resistance at high temperatures. Hypereutectic alloys are extensively used by German manufacturers for the production of heat resisting components in combustion engines.

Al-Si alloys are frequently treated to obtain enhanced mechanical properties in as-cast conditions. The most commonly applied treatments are sodium and strontium modifications. Transference of small quantities of these elements into melt under controlled conditions is known to change aluminum-silicon irregular flake structure into fibrous-type structure, which behaves like a fibre reinforced composite and leads to enhanced mechanical properties [1]. However, these methods have some disadvantages, as well, such as high volatility, gassing and rapid rate of burn-out of Na and Sr. Moreover, these elements are also known to increase the viscosity of Al-Si alloys, thus reducing

the fluidity of the charge in casting process.

Recently, antimony modification has found considerable application as an alternative tool of refining the structure of Al-Si castings. It has been semi-quantitatively reported that antimony treatment provides a permanent refinement of the structure [2]. Moreover, its refining effect is reported to be totally unaffected by the length of time through which the charge is kept in the liquid state, following remelting or degassing. However, despite its widespread applications in recent years, there seems to exist little information on the aspects of antimony treatment of Al-Si eutectic alloys.

The work described in this thesis is concerned primarily with the modification of Al-Si eutectic alloys by antimony additions. Microstructure and mechanical properties of antimony treated Al-Si alloys were investigated. It was found that structural refinement and mechanical properties of Al-Si eutectic alloy reaches a maximum at 0.1 wt % of antimony and the structure gets coarser at higher concentration levels. Besides, the effect of growth variables were observed in detail on the microstructure and mechanical properties both in unmodified and modified structures.

II. LITERATURE REVIEW

2.1 INTRODUCTION

Eutectic solidification has been the subject of considerable investigations in the past decade. Much of the attention have been paid to the study of kinetics and mechanism of eutectic growth. Also attention has been focused upon the structural aspects as modification of eutectic structure with particular reference to sodium and strontium treatments. Despite these efforts, little systematic work has been carried out on antimony modification. This chapter is hoped to present a reasonable background for the modification of aluminum-silicon castings for the reader.

2.2 ASPECTS OF EUTECTIC GROWTH

2.2.1 Definition and Classification of Eutectic Structures

An eutectic point occurs at the intersection of two liquidus lines, that slopes are in opposite directions, which is at a fixed temperature and composition and the liquid is in equilibrium with two different solid phases as illustrated in Figure 2a. Different classifications of eutectic microstructures have been proposed. Scheil's [3] original terminology was normal, anomalous and globular.

Normal structures display lamellar (Figure 1a) or rod (Figure 1b) morphologies and occur in systems with a symmetrical phase diagram (Figure 2a), whereas anomalous structures like the aluminum-silicon flake morphology (Figure 1c) has been associated with an asymmetrical phase diagram (Figure 2b). Details of each of these structures were presented in Table 1.

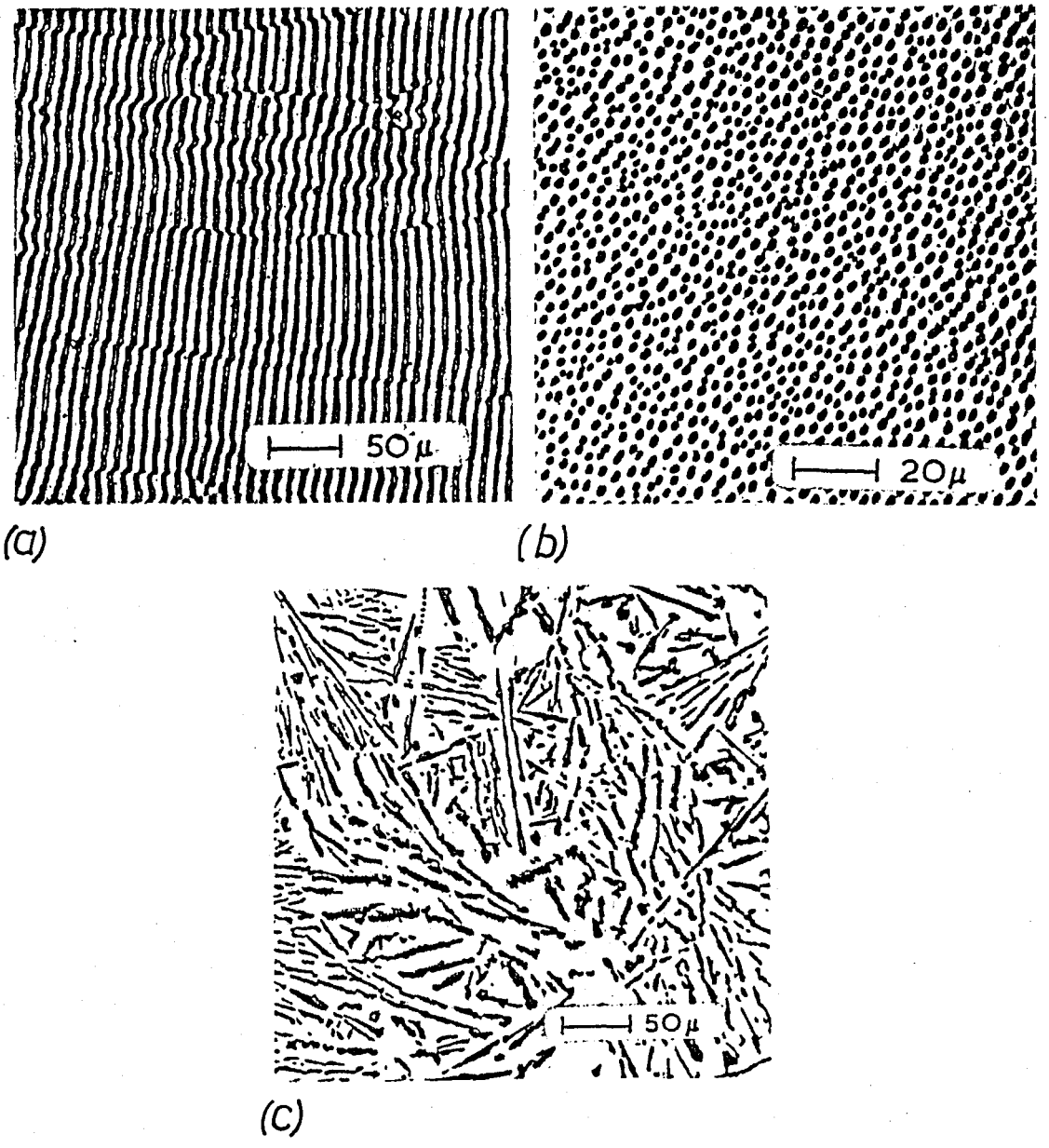

Figure 1 - Eutectic morphologies
(a) Lamellar morphology, (b) Rod morphology
(c) Anomalous flake morphology

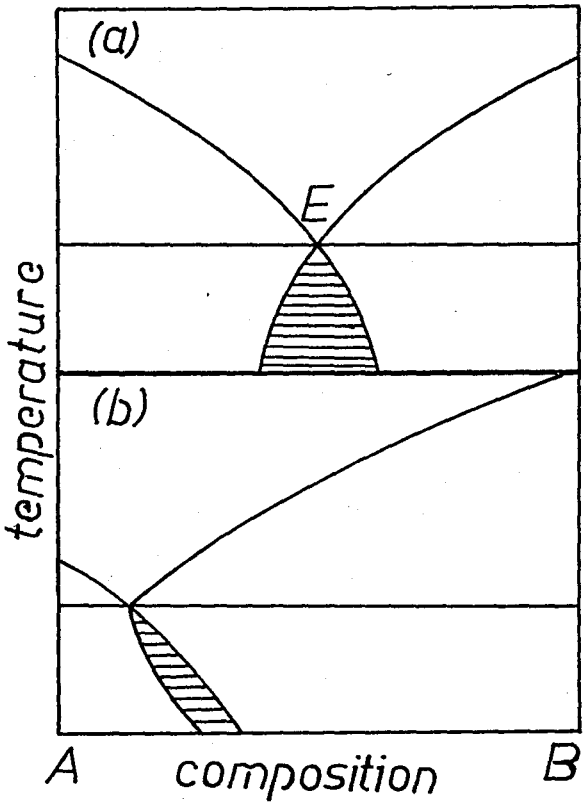

Figure 2 - Phase diagrams for normal and anomalous structures

a) Symmetrical phase diagram and coupled zone associated with a normal structure;

b) Asymmetrical phase diagram and coupled zone associated with an anomalous structure.

Eutectic microstructures can also be classified according to the growth characteristics of the component phases. These are non-faceted-non-faceted, non-faceted-faceted and faceted-faceted groups [4].

The non-faceted-non-faceted mixtures give regular lamellar or fibrous microstructures. These eutectic systems are usually produced when both eutectic phases have a low entropy of fusion. Both phases grow continuously and exhibit no faceting.

The non-faceted-faceted eutectic mixtures give rise to irregular or complex-regular morphologies. Al-Si alloy system falls into this

TABLE 1 - Classification of Eutectic Structures

1. Normal Structures:

   a. *Lamellar:* An arrangement of plates which is spacially regular over large distances, but usually containing intersecting faults.

   b. *Rod :* This is the same as lamellar structure but the rods may be polygonal in cross-section.

2. Anomalous Structures:

   a. *Irregular:* The spatial arrangements such as isolated unbranched and branched plates are not regular over large distances. At low growth velocities, these may include massive well-faceted particles.

   b. *Broken lamellar:* A near-regular array of broken plates.

   c. *Fibrous :* An array of interconnected fibres of low aspect-ratio, which may sometimes display microfacets.

   d. *Complex-regular:* An array of plates or fibres which are regular over small areas, usually form as a result of growth with a macro faceted projection at the solid/liquid interface.

   e. *Chinese script:* An array of discrete, finely branched sheet of the faceting minor phase in a non-faceting matrix plane.

   f. *Quasi-regular:* An array of sheet and/or fibres of an non-faceting minor phase in a matrix of a high entropy phase.

The notation used by Chadwich [4] was continuous, discontinuous and spiral. The first two groups related to phase continuity in the growth direction.

category, because the silicon rich phase has a high entropy of melting and is therefore likely to solidify with an atomically smooth or faceted interface, while the aluminum-rich phase has a low entropy of fusion and will therefore solidify with an atomically rough interface.

The faceted-faceted regime results in microstructures which are merely very fine aggregations of independent crystals of the two components growing cooperatively.

2.2.2 Growth in Normal Eutectic Structures

In the past few years many studies have been made in understanding the growth behaviour of eutectic phases. In general, it has been found that the growth morphology developed by a eutectic system is governed by the growth characteristics of the individual constituents. This behaviour is related to the nature of the solid-liquid interface and can be predicted for pure materials from the entropy of fusion value.

Jackson [5] predicted the structure of the solid-liquid interface of a material in contact with its liquid using the α factor which is closely related to the entropy of fusion ΔS_f by the equation

$$\alpha = \frac{L_o}{k\ T_E}\ (\eta/u) \approx \Delta S_f(\eta/u)$$

where, η is the number of nearest neighbours of an atom which is on the same plane at the solid-liquid interface, u is the coordination number, L_o is the latent heat of fusion, k is Boltzmann's constant and T_E is the melting temperature. A statistical mechanical analysis showed that if $\alpha > 2$ the solid-liquid interface is atomically smooth

and advances into the liquid by the propagation of atomic steps across the interface. This growth process requires considerable kinetic undercooling.

Twin plane re-entrant edges (TPRE) are present in many anomalous eutectics and provide a continuous supply of atomic steps on the interface during growth.

When $\alpha < 2$ the solid-liquid interface is atomically rough and it has been observed that many sites are readily and continuously available for atomic attachment during growth. Such an interface advances normal to itself with little kinetic undercooling and fast enough for other factors to limit the growth rate.

Each phase of a normal or regular structure has a low entropy of solution and after nucleation grows with a rough interface requiring little kinetic undercooling. Lamellar and rod structures form under these conditions.

The interlamellar or inter rod spacing is determined as a result of a balance between a tendency to minimize the interlamellar spacing and an attempt to increase it in order to reduce the solid-liquid interfacial area, hence the energy per unit volume of the eutectic [6].

The most comprehensive treatment of this balance is done by Hunt and Jackson [5]. Their analysis considers the solid-liquid interface to be undercooled by an amount ΔT during steady-state growth where,

$$\Delta T = \Delta T_D + \Delta T_C + \Delta T_K$$

The contribution ΔT_D is due to the compositional differences that must exist across the interface because of the necessity of

transporting material from in front of one solid phase to the liquid ahead of the other. This contribution is calculated from the relationship

$$\Delta T_D = m_L(C_E - C)$$

where, m_L is the liquidus-slope, C_E is the eutectic composition, and C is the local liquid interface composition obtained from the solution of the diffusion equation. ΔT_C is defined by

$$\Delta T_C = a/r(x)$$

where, a is a constant given by the Gibbs-Thomson relationship and r(x) is the local curvature of the interface. Both of these terms relate to changes in the local equilibrium temperature from the equilibrium eutectic temperature and can be obtained from the thermodynamics of an equilibrium system.

The contribution of the kinetic undercooling ΔT_K is considered to be negligibly small for non-faceting-non-faceting systems.

Hunt and Jackson [5] obtained an analytical solution by approximating the interface composition to that on a plane interface and presented solution by separating variables was of the form,

$$C = C_E + C_\infty + B_o \exp(-\frac{R}{D} z) + \sum_{n=1}^{n=\infty} B_n \cos(\frac{n\pi x}{S_\alpha + S_\beta}) \exp(-\frac{n\pi x}{S_\alpha + S_\beta}) \qquad (1)$$

where C_E is the eutectic composition, C_∞ is the composition far away from the interface, R is the growth velocity, D is the diffusion coefficient.

S_α and S_β are the half-widths of the α and β lamellae.

$$\lambda = 2(S_\alpha + S_\beta)$$

z is the distance in the growth direction and x is the position across the surface, (Fig. 3)

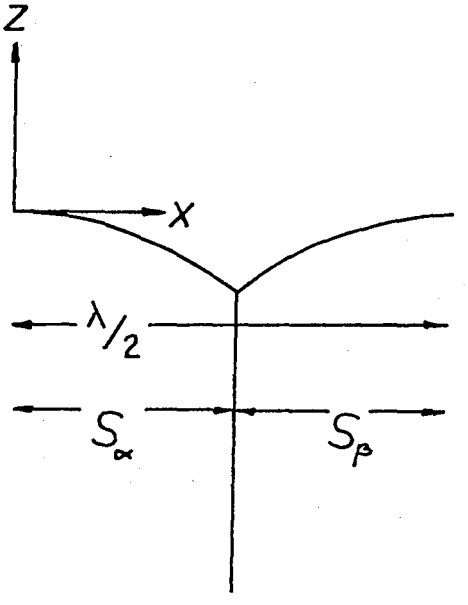

Figure 3 - The definitions of z, x, S_α, S_β and λ

Equation (1) gives an average interface composition of $C_E + C_\infty + B_0$ which differs from the eutectic composition. This composition difference allows both phases to grow at one temperature although they have very different surface energies or liquidus slope.

The coefficients B_0, B_n may be evaluated using the continuity of matter equation at the interface

$$B_o = \frac{\bar{C}_o^{\alpha} S_{\alpha} - \bar{C}_o^{\beta} S_{\beta}}{S_{\alpha} + S_{\beta}}$$

$$B_n = \frac{2}{(n\pi)^2} (S_{\alpha} + S_{\beta}) \frac{R}{D} (\bar{C}_o^{\alpha} + \bar{C}_o^{\beta}) \sin \frac{n\pi S_{\alpha}}{S_{\alpha} + S_{\beta}}$$

$\bar{C}_o^{\alpha}$ and $\bar{C}_o^{\beta}$ are the average differences between the solid and liquid on each of the phases.

The average diffusion undercooling may be calculated using Equation (1) and when combined with the average undercooling due to curvature gives average total undercoolings for each of the phases;

$$\Delta T_{\alpha} = m_{\alpha}[C_{\infty} + B_o + \frac{2R}{D} C_o (\frac{S_{\alpha} + S_{\beta}}{S_{\alpha}})^2 P] + \frac{a_{\alpha}^L}{S_{\alpha}} \qquad (2)$$

and

$$\Delta T_{\beta} = m_{\beta}[-C_{\infty} - B_o + \frac{2R}{D} C_o (\frac{S_{\alpha} + S_{\beta}}{S_{\beta}})^2 P] + \frac{a_{\beta}^L}{S_{\beta}} \qquad (3)$$

where, m_{α} and m_{β} are the liquidus slopes of the α and β phases, C_o is the length of the eutectic horizontal, a_{α}^L and a_{β}^L are surface energy terms and P is a tabulated function of S_{α}/S_{β}.

Equations (2) and (3) can be equated for an isothermal interface and the coefficient B_o is eliminated but as B_o varies with the ratio $S_{\alpha}/S_{\beta}(\xi)$ the resulting equation applies for a particular value of (ξ), i.e. the equilibrium value. The resulting equation is;

$$\frac{\Delta T}{m_L} = R\lambda Q^L + \frac{a^L}{\lambda} \qquad (4)$$

where,

$$1/m_L = 1/m_\alpha + 1/m_\beta \quad , \quad Q^L = \frac{P(1+\xi)^2}{D\,\xi} C_o$$

and

$$a^L = 2(1+\xi)\left[\frac{a_\alpha^L}{m_\alpha} + \frac{a_\beta^L}{\xi m_\beta}\right]$$

and

$$\lambda = 2(S_\alpha + S_\beta)$$

The evaluation of the coefficients in these equations requires a knowledge of the average composition differences between the solid and liquid on each phase. For a given value of growth velocity, equation (4) has a minimum point where,

$$\lambda^2 R = a^L/Q^L = \text{const.}$$

and

$$\Delta T^2/R = 4m_L^2 a^L Q^L = \text{const.}$$

The second form of normal structures often observed is the rod-morphology. Rod growth has been analysed in a manner similar to lamellar growth [7].

The equations are also similar except that the cosine series are replaced by Bessel function series. A general equation is produced of the same form as equation (4).

$$\frac{\Delta T}{m_L} = RTQ^T + \frac{a^T}{T} \qquad (5)$$

where, T is the rod spacing.

$$a^T = 2(1+\xi)^{1/2}\left[\frac{a_\alpha^T}{m_\alpha} + \frac{a_\beta^T}{\xi m_\beta}\right]$$

$$Q^T = \frac{4(1+\xi)}{D\,\xi} C_o M$$

where a_α^T and a_β^T are surface energy terms and M is a tabulated function of the volume fraction [9]. Equation (5) requires a further boundary condition in order to define a unique relationship between T, ΔT and R. It is usually assumed that the structures grows with the extremum spacing. This gives;

$$RT^2 = a^T/Q^T$$

$$\Delta T^2/R = 4m_L^2 a^T Q^T$$

It is also found by comparing the undercoolings for lamellar and rod structures that, rod should grow when the following condition is satisfied;

$$\frac{\left[\frac{a_\alpha^L}{m_\alpha} + \frac{a_\beta^L}{m_\beta}\right]}{\left[\frac{a_\alpha^T}{m_\alpha} + \frac{a_\beta^T}{m_\beta}\right]} > \frac{4m_L}{P} \frac{1}{(1+\xi)^{3/2}}$$

If the solid-liquid and α-β free energies are the same for both structures the inequality is simplified and the left hand side becomes equal to one.

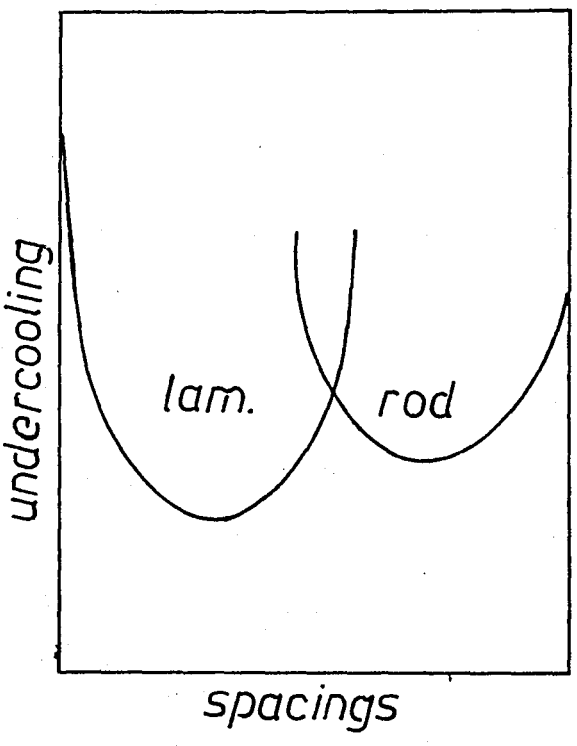

Figure 4 - Relationship between interface undercooling and interphase spacing for lamellar and rod growth.

2.2.3 Growth in Irregular Eutectic Structures

An irregular eutectic is the one in which one of the phases must renucleate repeatedly owing to the termination of growth of crystals of that phase. The discontinuity of the eutectic is apparently as a result of a very specific morphology of the crystals of the discontinuous phase which nucleate with random orientations and therefore grow in directions which are randomly oriented with respect to the growth interface [8].

This leads to a situation shown schematically in Figure 5, in which three silicon crystals A, B and C are shown, growing to the right as the interface I advances.

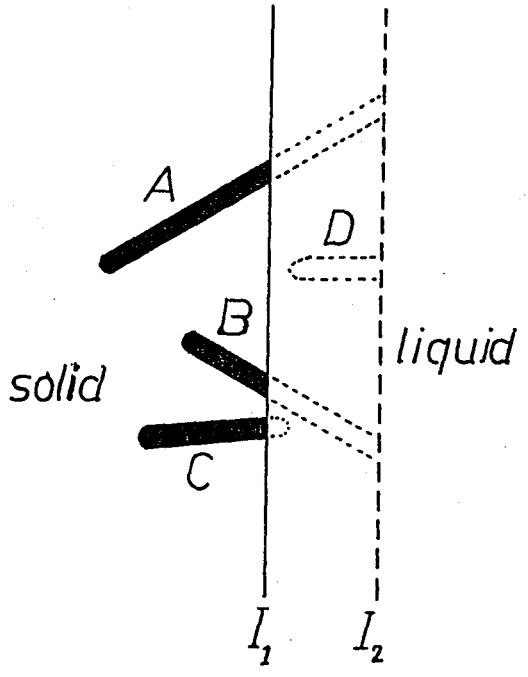

Figure 5 - Growth of a discontinuous eutectic [8]

The distance between A and B increases with the result that, the silicon concentration in that region eventually reaches a level at which nucleation of a new crystal D occurs. In the same way crystal C stops growing because it is in competition with B for silicon. The general explanation of discontinuity in irregular eutectics is therefore the existence of strong anisotropy in the growth characteristics of one of the phases.

Another approach for the growth of Si phase can be explained with the undercooling below the equilibrium eutectic temperature [1]. When a non-faceted-non-faceted eutectic freezes, the undercooling below

the equilibrium eutectic temperature ΔT is given by equation (4). This equation can be rewritten as

$$\Delta T = V\lambda A + B/\lambda \qquad (6)$$

where λ is the lamellar spacing, V is the velocity, A and B are constants. Equation (6) can be plotted for a given growth rate (Fig. 6). It has been shown for non-faceted-non-faceted eutectic alloys that the eutectic grows at or near the minimum undercooling [1], while in a faceted-non-faceted eutectic such as aluminum-silicon, it is suggested that eventhough the structure is irregular, an expression similar to above equation is still valid [1]. The very large spacing and total undercooling found in this system are consistent with growth at a much larger spacing than the minimum undercooling spacing.

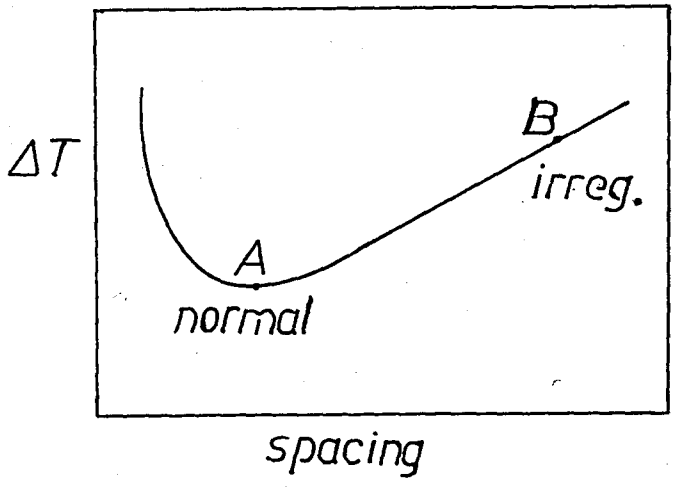

Figure 6 - Schematic plot of undercooling vs spacing for faceted-non-faceted growth.

The much larger spacing in such cases, has been attributed silicon plates growth at an angle to one another; as two plates grow together one of them will block off the other. The average spacing will be determined by the ability of the silicon to branch or produce new plates to fill the gaps. If branching is difficult, the average spacing will become very large. If branching is easy, the spacing should approach the minimum undercooling value. The large undercoolings found in aluminum-silicon eutectic alloys are thus attributed to the diffusion term $AV\lambda$. A kinetic undercooling term might also be included to allow for the kinetic undercooling of the faceted silicon phase. However, this will be small compared with the diffusion term and the total undercooling.

2.2.4 Microstructural Analysis of Aluminum-Silicon Eutectics

The growth variables were found greatly to affect the mode of the eutectic reaction and to cause not only changes in the scale of the eutectic microstructure but to alter the form of the microstructure as well. Various microstructures from the unidirectional solidification experiments were therefore classified in terms of varying G_L and R in the ranges from $1^{o}C/cm$ to $1000^{o}C/cm$ and from $1x10^{-5}$ cm/sec to $1x10^{-1}$ cm/sec respectively as in Figure 7.

It was shown that the matrix never exhibited any growth texture, except when primary α-Al dendrites were present then the expected <100> aluminum growth texture was observed. It was also shown that no consistent orientation relationship existed between the matrix and the

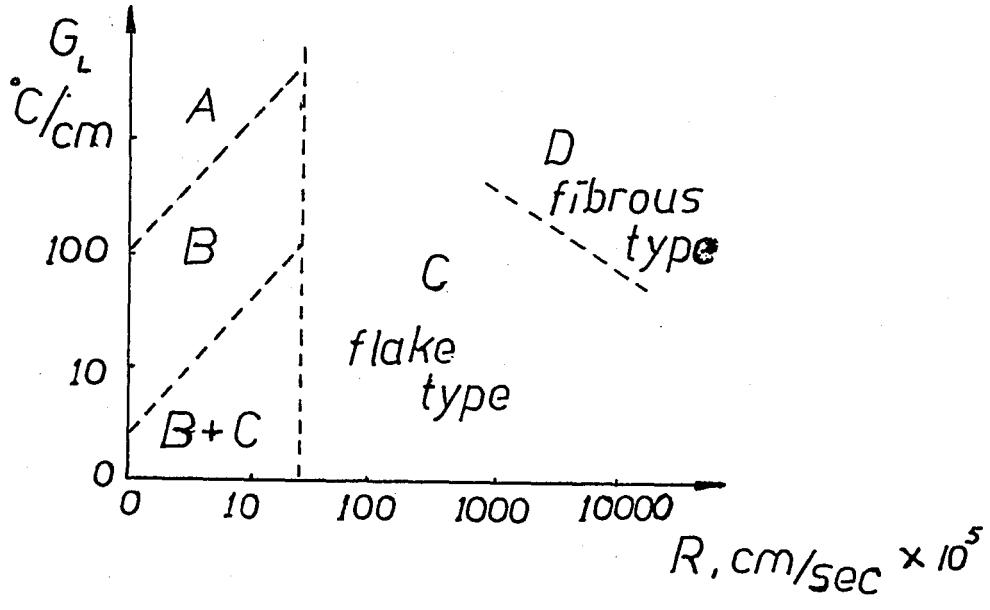

Figure 7 - G_L/R plot for Aluminum-Silicon eutectic alloys showing the distinct growth regions A, B, C and D [11]

silicon crystals. In all these alloys the metallic phase may be regarded as an isotropic matrix which contains a wide range of silicon particles which characterize the microstructure.

The characteristic regions will therefore be discussed in terms of the silicon microstructure. The structure produced in region A of the G_L/R plot was one in which a relatively long range diffusion process produced massive crystals of the two eutectic phases [11]. This region of the G_L/R plot was delined by a parameter of high temperature gradient in the liquid at the interface, G_L and low growth rate, R. Above this critical G_L/R value the eutectic silicon consisted of large faceted crystals roughly aligned with the growth direction.

Aluminum phase grows with a planar interphase. Local growth directions of silicon crystals were either <100> or <211> and the crystals were heavily {111} twinned and interconnected. The silicon appeared to be growing by a twin-plane re-entrant edge mechanism (TPRE) and greatly resembled silicon dendrites grown from silicon melts.

This massive structure was produced because the high G_L/R values were sufficient to prevent constitutional supercooling of the aluminum phase by the silicon.

The aluminum therefore grew with a planar interface, making the formation of a long range diffusion front between the two phases very difficult to achieve and so a massive structure was formed.

In region B, the planar aluminum interface became unstable and formed cells. The eutectic silicon then occurred as rods, which were aligned in the growth direction and had a <100> silicon growth texture. Diffusion distances were reduced by an order of magnitude and growth was assumed cooperative.

These rods tended to form a hexagonal array, when observed on a section transverse to the growth direction as if they were growing at aluminum-cell triple boundaries.

If the growth rate was kept constant and the temperature gradient successively decreased, the silicon rods developed axial side plates, the size of which varied inversely with the temperature gradient. The eutectic then appeared angular on a transverse section. Longitudinal sections showed the presence of wavy silicon crystals.

Side plates were of two types; either smooth or corrugated. It was the sections through corrugated plates that gave rise to the

wavy lines when these specimens were viewed longitudinally.

In this region of the G_L/R plot the silicon phase was growing by a mechanism that did not involve {111} twins, since these were shown not to be present. This is because the low undercoolings present at the silicon interface were not sufficient to produce these growth twins. The operative growth mechanism may well have involved screw dislocations present in the silicon crystals.

In regions B and C an increase in the growth rate caused a decrease in the size of the angular silicon particles and the concomitant formation of {111}, irregular silicon plates in between the angular particles. These irregular plates are interconnected and attached to the angular particles.

In region C, the growth rates were greater than $3x10^{-4}$ cm/sec and the entire specimen was in the irregular form.

The growth conditions normally found in castings fall in this region of the G_L/R plot and so the non-steady state irregular form is the one usually observed.

Irregular plates are {111} and contained {111} twins. It was the presence of these twins that gave rise to the apparently random array of silicon crystals. The crystals being interconnected and related to each other by multiple twinning operation.

The operative growth mechanism in this region of the G_L/R plot is also related to the presence of {111} twins. Silicon growth takes place preferentially from twin-plane re-entrant edges. For continued growth to occur more than one twin plane is necessary. The average spacing, λ between silicon particles was found to decrease as growth rate is increased.

In region D, the growth rate exceeded a certain value the structure was changed from irregular {111} plates to an increasingly convoluted and fibrous form. This transition in morphology was continuous and eventually the microstructure became that of the quenched alloy.

2.2.4.1 Coupled Growth

At temperatures below the eutectic temperature, it is possible to freeze liquids covering a wide range of composition into solids having a eutectic micromorphology and which grow with a stable planar interface. The region of stable cooperative growth below the eutectic temperature has been termed the "coupled region" or "coupled zone".

Although the nominal eutectic composition is 12.6 wt%. Silicon, Al-Si alloys with silicon concentrations in the range 12-20 wt% contain primary aluminum or primary silicon in proportions depending upon both composition and freezing rate. Primary aluminum was easily identified as dendrites which were generally coaxial with the specimen. Primary silicon occurred as feathery crystals. But in alloys well away from the coupled zone, i.e. at high silicon contents, these growth forms thickened into relatively massive silicon needles [12].

There is a narrow band of composition and growth rates in which neither primary phase could be detected (Fig. 8). The microstructure in such specimens was that of a eutectic but the volume fraction of silicon was variable.

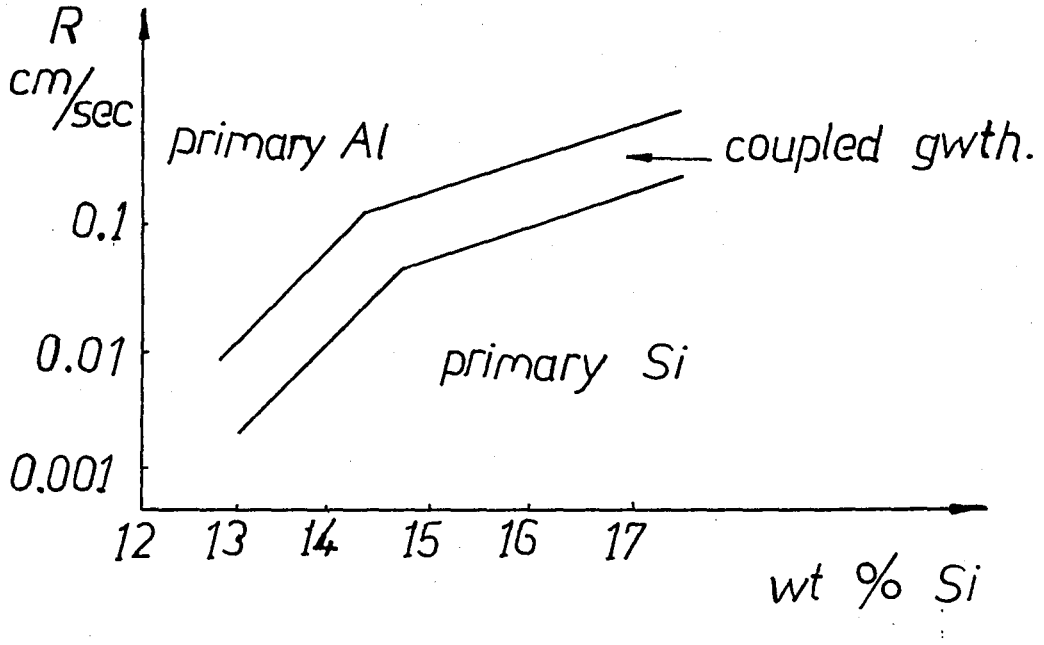

Figure 8 - Incidence of primary aluminum, primary silicon and coupled growth in directionally solidified Al-Si alloys [12].

The results suggest a change in slope of the coupled region over a velocity range between approximately 400 and 1000 μm/sec but it is not clear whether this should be a sharp or a gradual inflexion.

The range of coupled growth increases as the undercooling increases.

At all positions within the coupled zone, the two phases are able to grow cooperatively by the normal short range diffusional mechanism at a rate exceeding that of either of the component phases. Thus, when the primary phases are nucleated within the coupled zone, free dendritic growth is soon stifled; because, the eutectic material quickly engulfs them. Outside the coupled region, one primary phase first grows

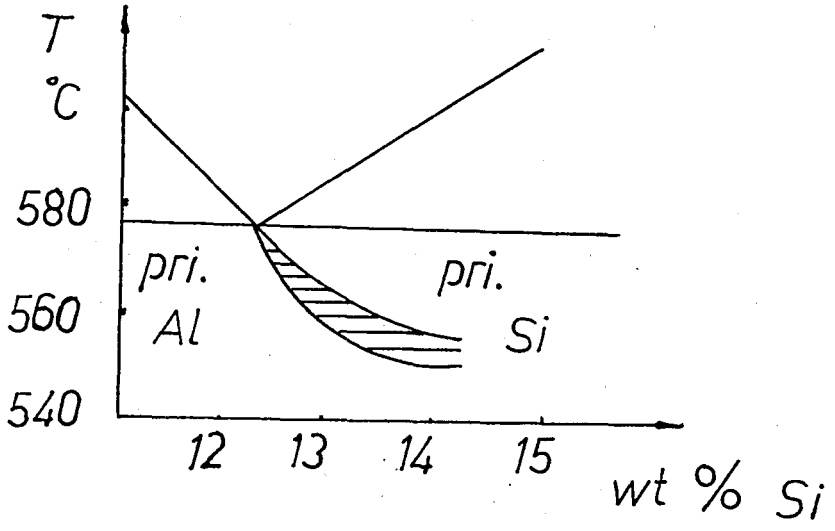

Figure 9 - Incidence of primary phases and coupled growth in terms of temperature and composition in Al-Si alloys.

until the liquid is enriched sufficiently in the other component to allow eutectic growth.

Primary aluminum dendrites are often found in castings of eutectic alloys, because of the difficulties involved in nucleating the silicon phase. Primary-phase dendritic growth of eutectic alloys can be suppressed during unidirectional growth if the temperature gradient ahead of the interface is sufficiently steep.

For each alloy composition these exists a critical value of G_L/R above which stable planar growth is possible and below which the interface is unstable and dendritic growth of the primary phase

can take place. The critical condition can be stated analytically as,

$$G_L/R \geq - \frac{m_L(C_E - C_o)}{D} \qquad (7)$$

where, m_L is the slope of the liquidus line at the eutectic composition, C_E and C_o are the compositions of the eutectic and the starting alloy respectively, D is the liquid diffusion coefficient.

Since m_L, C_E and D are constant for a certain alloy system. The critical condition for planar-dendritic breakdown is linear with composition. Also, it is evident from Figure 10 that the width of the coupled zone increases with increasing temperature gradient.

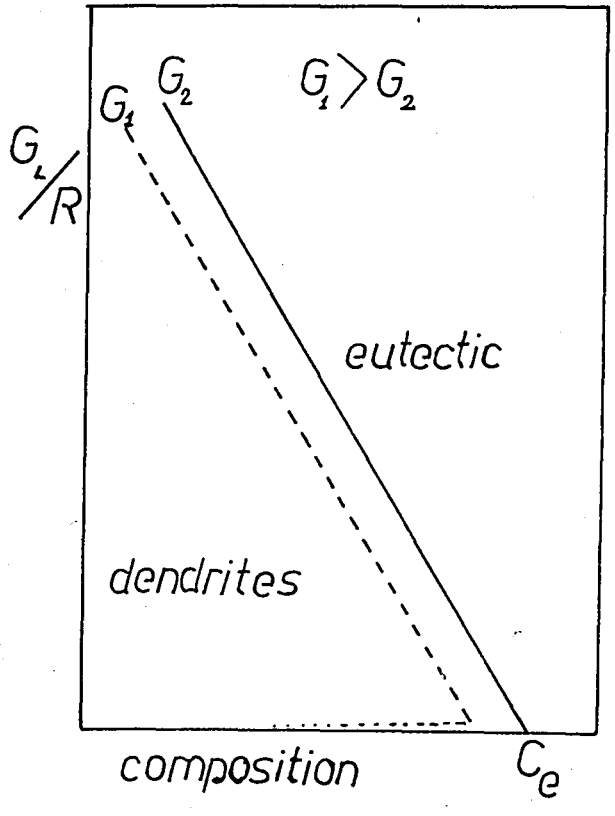

Figure 10 - Schematic representation of dendrite-eutectic transition as a function of G_L/R.

2.3 MODIFICATION of Al-Si EUTECTIC ALLOY

Aluminum-silicon foundry alloys are frequently treated to obtain a fine eutectic structure in order to have optimum mechanical properties especially in toughness in as-cast or heat treated castings. The popularity of aluminum-silicon alloys as casting media stems from the discovery of Pacz [13] that a marked improvement in the mechanical properties of this alloy could be detected by the addition of a small quantity of alkali fluorides to the melt before casting.

The increase in ductility upon modification is principally due to a reduction in the coarseness (i.e. refining) of the silicon phase, since it has recently been shown that, the cracking of silicon particles in an aluminum matrix occurs progressively over the range of plastic deformation of the alloy. The fracture probability of any silicon particle increases with increasing particle size and decreasing silicon content. Also, the growth process is affected in such a way that, primary dendritic growth occurs in what is nominally an alloy of eutectic composition.

2.3.1 Conventional Modification Methods of Al-Si Eutectic Alloys

The treatments most commonly used are sodium and strontium modifications. These modifiers are very efficient in converting the coarse acicular or (irregular plate-type) eutectic structure into a fibrous eutectic structure. Russian workers have been particularly concerned with the changes induced in liquid aluminum-silicon alloys by modifying addition. Some of this work has been reviewed by Korol'kov [14].

He considered that, metals which considerably reduce the surface tension of liquid aluminum or aluminum-silicon alloys should be effective modifying agents. In agreement with these predictions, it is found that lead and bismuth both reduced surface tension and also modified the aluminum-silicon eutectic structure. However, Kim and Heine [14] could obtain no modification with these elements. These workers have examined the effect of various other metals on the refinement of the eutectic and found that elements in Group 1A of the periodic table, with the exception of lithium were effective modifying agents, sodium being the most effective for a given addition.

Kim and Heine also noted that, the element must be capable of being added at a suitable high temperature to ensure adequate dispersion. In particular, they consider that many of the Al-group 1A system have a miscibility gap at lower temperatures which hinders dispersion. However, high temperatures favour volatilization of the addition and lead to the well known effect of fading, i.e. gradual inability to modify on holding the alloy in the liquid state or on remelting.

Because of the founding difficulties associated with fading the effect of various additions have recently been reexamined [14]. Sodium was found to fade badly. Cerium and Rubidium also faded quickly. Potassium and lithium produced little modification. Calcium and barium, although forming packets of modification, gave poor flow characteristics and an increased tendency to oxidation. The effect of strontium was remarkable. Not only to have a refining effect comparable with that of sodium but it showed very little fading, the modification lasting for several hours in the liquid alloy. Besides

these elements, the use of antimony to refine the eutectic is a recent development. Its advantage is that the antimony is a permanent constituent of the alloy. Its refining effect is completely unaffected by holding time, remelting or degassing.

Sodium Modification

Sodium modification for the aluminum-silicon alloys is an important mechanism and it will be beneficial to clarify this modification mechanism before the explanation of antimony modification. The addition of only 0.01 wt% sodium produces a change in the silicon particle spacing and the morphology of the silicon changes from a plate-like to a branched fibrous form (Figure 11).

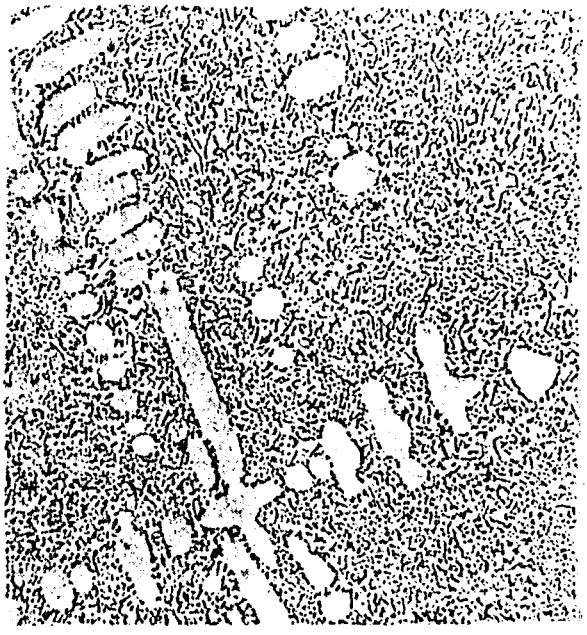

Figure 11 - Sodium-modified Al-Si eutectic morphology.

There have been two main types of explanation for the sodium modification process. Some favours that point of view based on sodium affecting the nucleation of the silicon phase and others support the idea of sodium affecting the growth of the silicon. Day [11] has confirmed that this modified structure was the result of a change in the mode of growth and not the result of a change in nucleation behaviour. Unidirectional growth experiments with sodium-doped Al-Si eutectic showed that sodium modified the irregular structure in region C of the G_L/R plot in Fig. 7, but not the angular structure in region B of the G_L/R plot. The most obvious mechanism of Na modification would seem to be the poisoning of re-entrant {111} twin grooves. Day and Hellawell [15] have proposed that selective absorbtion at such sites will retard the growth of Si and increase the interface undercooling, leading the more frequent overgrowth by the Al-phase and more twin formation. A high twin population, which has been detected in fibrous structure, allows frequent branching. Fredriksson [16] has shown that although twinning frequency increases, there is doubt as to whether this continues with increasing impurity content and undercooling. Observations made by Gigliotti and Colligan [14] have also been in terms of a change in the crystal growth habit of the silicon-phase. Recently, Hunt and Flood [1] proposed that Na does not only alter the growth behaviour of silicon-phase but also prevents nucleation occurring ahead of the eutectic growth front, which was responsible for the refinement of the structure and caused larger undercooling.

Although kinetic factors control the growth morphology, Davies and West [15] has been reported that the influence of sodium additions

on surface tension and interphase boundary energy should not be ignored. Sodium was presumed to be surface active on the growing silicon by reducing its interfacial energy about 25% at a sodium concentration of 0.1 wt%.

Finally, accumulation of sodium at the solid-liquid front is compatible with the subsequent overmodification bands which occur with increasing sodium content [1].

2.3.2 Antimony Modification of Al-Si Alloys

The development of a permanent modifying agent has been the object of considerable research. In the past few years antimony has found considerable attention as a permanent modifier of the aluminum-silicon eutectics [2]. As it was shown by Bliznakov and Yaneva [17] the effect of impurity adsorption on crystal growth and dissolution is symmetric. This permitted to make some conclusions about the effect of antimony on the growth of the silicon phase in aluminum-silicon alloys. It is suggested that, antimony addition retards silicon growth process during the solidification [17].

The refinement of structure can be connected with an undercooling rise at the solid-liquid interface due to the reduced growth of silicon particles to large sizes. According to Hansen and Anderko [18], antimony is insoluble in solid silicon and is rejected into the melt during the growth. Thus a layer of relatively high antimony concentration builds up ahead of the solidification front, leading to additional undercooling. This makes the nucleation of new silicon particles and results the refinement of microstructure. Besides, for

a given solidification rate it has been found that the phosphorus content is a critical factor in determining the amount of a modifier required to produce the desired structure [2]. Antimony neutralizes the phosphorus as in the case of sodium and strontium. It does not, however confer a fibrous structure to the eutectic. The neutralization of the phosphorus has been explained by a mechanism similar to those advanced for sodium and strontium [2]; the antimony completely combines with the magnesium present to form the compound Mg_3Sb_2 which in turn, dissolves the phosphorus. In the absence of magnesium, AlSb, which has the same effect is formed.

So modification cause a depressed eutectic temperature therefore refining the microstructure and increasing the amount of primary aluminum-phase. Another important feature of the antimony modification mechanism found was that, at antimony additions higher than a certain amount, its concentration on the solid-liquid interface reached a critical value and nuclei of a new solid phase, Al-Sb, starts to form that leads to strong reduction of the antimony concentration in the layer ahead of the growing front. The effect of refinement diminishes and the silicon phase in the alloy gets coarser.

Advantages when compared with Sodium Modification

Antimony is a permanent constituent of the alloy. That means its modification is not affected by holding time of remelting. The disadvantages with sodium or strontium modifications are gassing and oxidation of the molten metal plus the tendency to produce a microporous castings. It is substantially eliminated when antimony

is used. Antimony based alloys are distinguished by their low susceptibility to gassing, excellent casting properties and the ability to produce sound castings. Besides, fluidity is not affected by antimony, thus enabling the production of thinner or more complex pieces than can be produced when sodium and strontium are used. Structure and mechanical properties are more reproducible due to antimony's permanence. Lost production time is reduced as there are no delays for remodification.

III. EXPERIMENTAL METHOD

3.1 EXPERIMENTAL PROGRAMME

In this present work, antimony modification of unidirectionally solidified aluminum-silicon eutectic alloys under steady-state conditions was investigated. The attention focused upon detecting the effect of antimony content, temperature gradient and growth rate upon the eutectic microstructure.

Mechanical properties of the unidirectionally solidified alloys were also examined.

3.2 APPARATUS

The apparatus used for unidirectional solidification was shown in Figure 12 and Figure 13. The system consists of a resistance heated vertical tube furnace, temperature controllers and a specimen drive system.

3.2.1 Growth Furnace

The growth furnace with the dimensions 14x14x30 cm had three separate heaters, each controlled independently by means of chromel-

alumel thermocouples inserted exactly in the center of the heating zone of each heaters, thermocouple leads being connected to Elimko control units. Another set of thermocouples were also inserted into the central location of each heater connected to the potensiometer. This set checks the value displaced on the control unit so that, more accurate measurements of the temperature could be made.

3.2.2 Drive System

The drive unit was used to move the specimen in the furnace at desired rates. It consists of a pulley system 1-10 cm in diameter and a winding pulley set $3/\pi$, $4/\pi$, $5/\pi$ cm in diameter. The output of motor was 2 rev/min and the output of the whole system could be varied in the range from 0.001 cm/sec to 0.148 cm/sec.

3.2.3 Growth Rods

For unidirectional solidification experiments, growth rods for both microexamination and mechanical testing were prepared by casting the metal into cylindrical steel molds, as shown in Figure 14. One of the mould had the dimensions of 100 mmx4 mm ϕ and used for preparation of growth rods for microexamination. The other had the dimensions of 100 mmx7 mm ϕ and used for the growth of mechanical testing specimens.

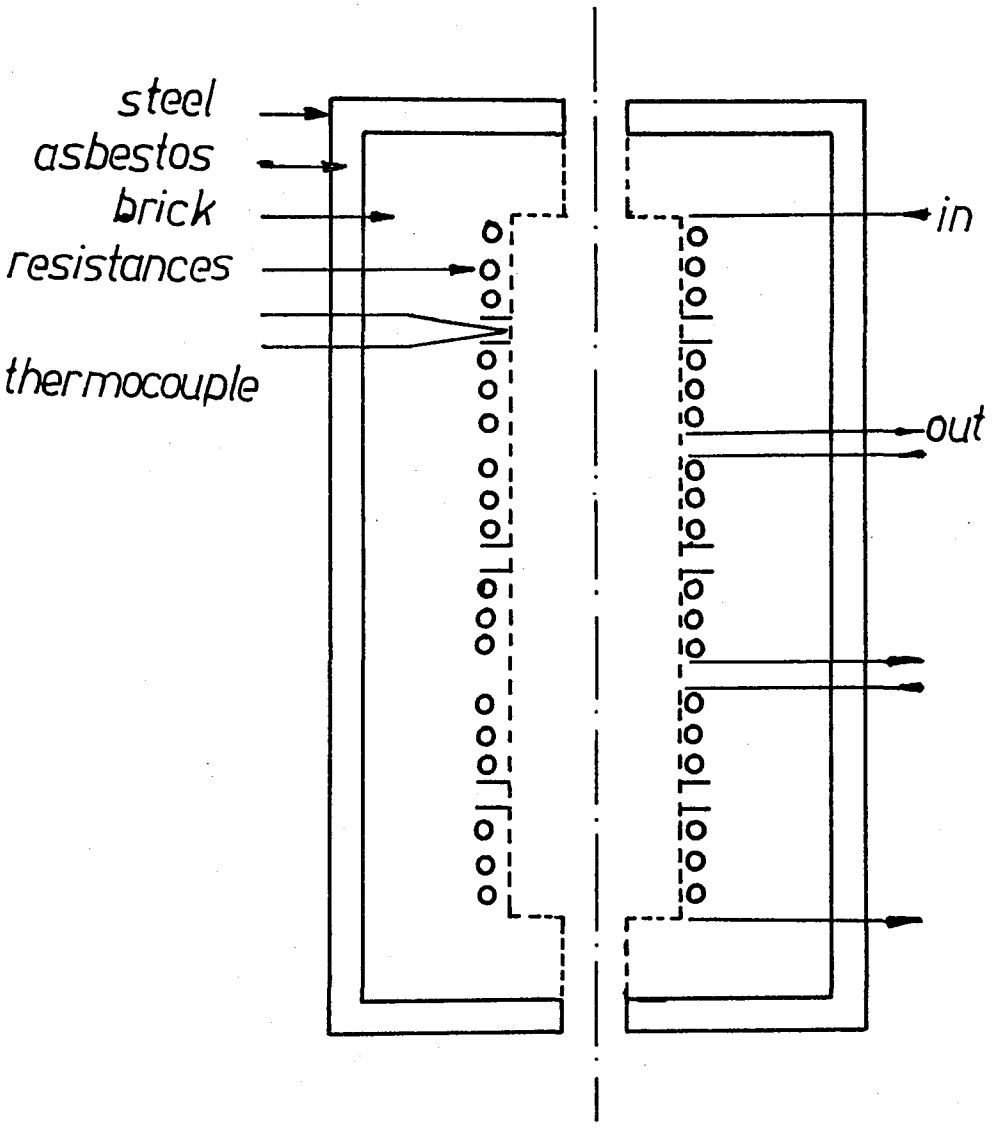

Figure 12 - Schematic view of the furnace.

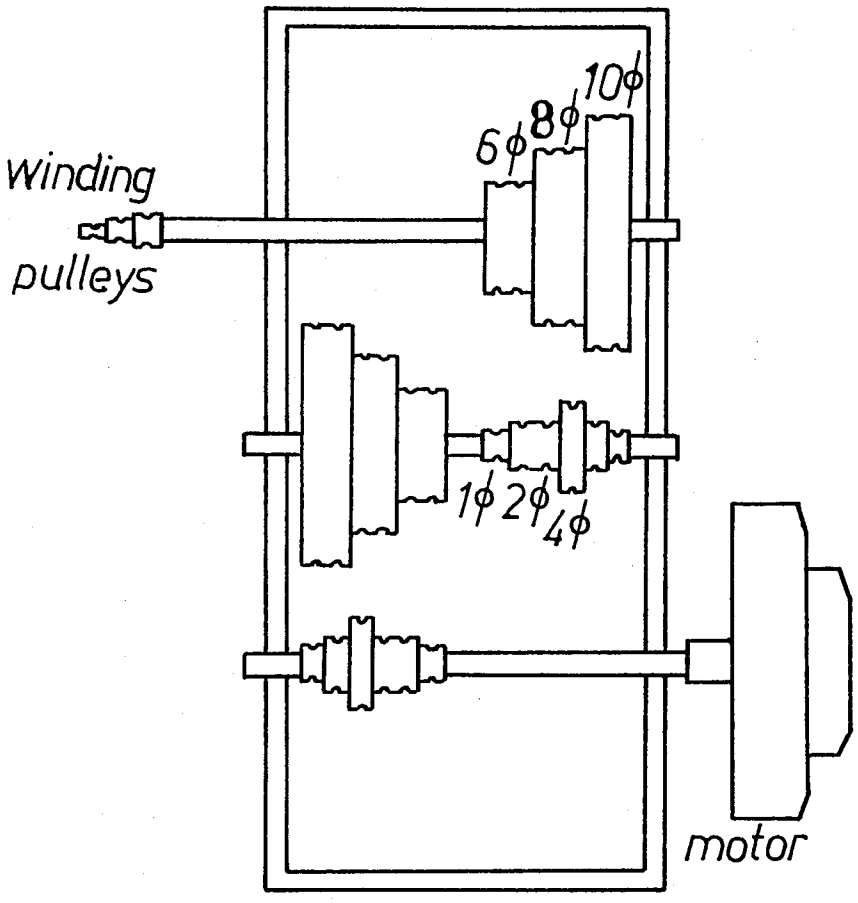

Figure 13 - Schematic view of the drive set.

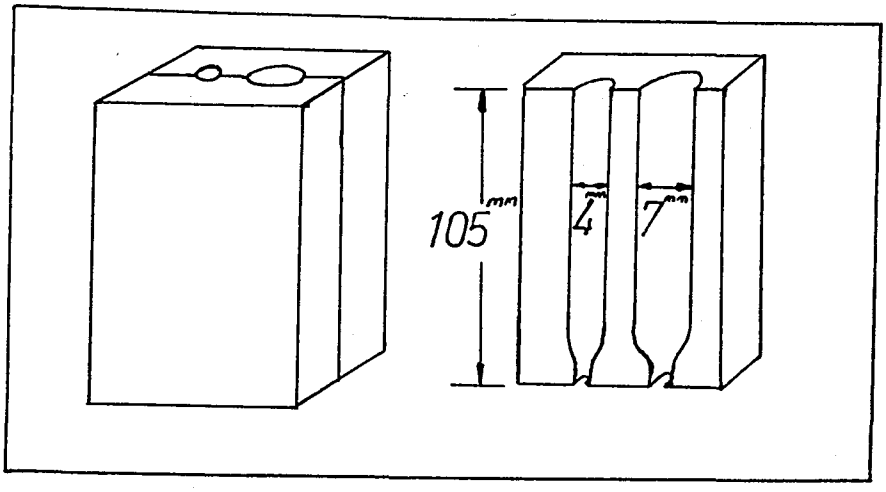

Figure 14 - Steel mould for growth rod preparation.

3.3 EXPERIMENTAL PROCEDURE

3.3.1 Alloy Preparation

Aluminum-silicon eutectic alloy (12.6 wt% Si) was prepared using 99.97% purity aluminum supplied by Alcan. The phase diagram of the Al-Si system is illustrated in Figure 15.

Accurately weighed amounts of aluminum and silicon were melted in a graphite crucible by means of a resistance heating furnace, then antimony was added into the molten charge, stirred with a graphite plunger to homogenize the melt composition and subsequently casted into the specimen preparation moulds.

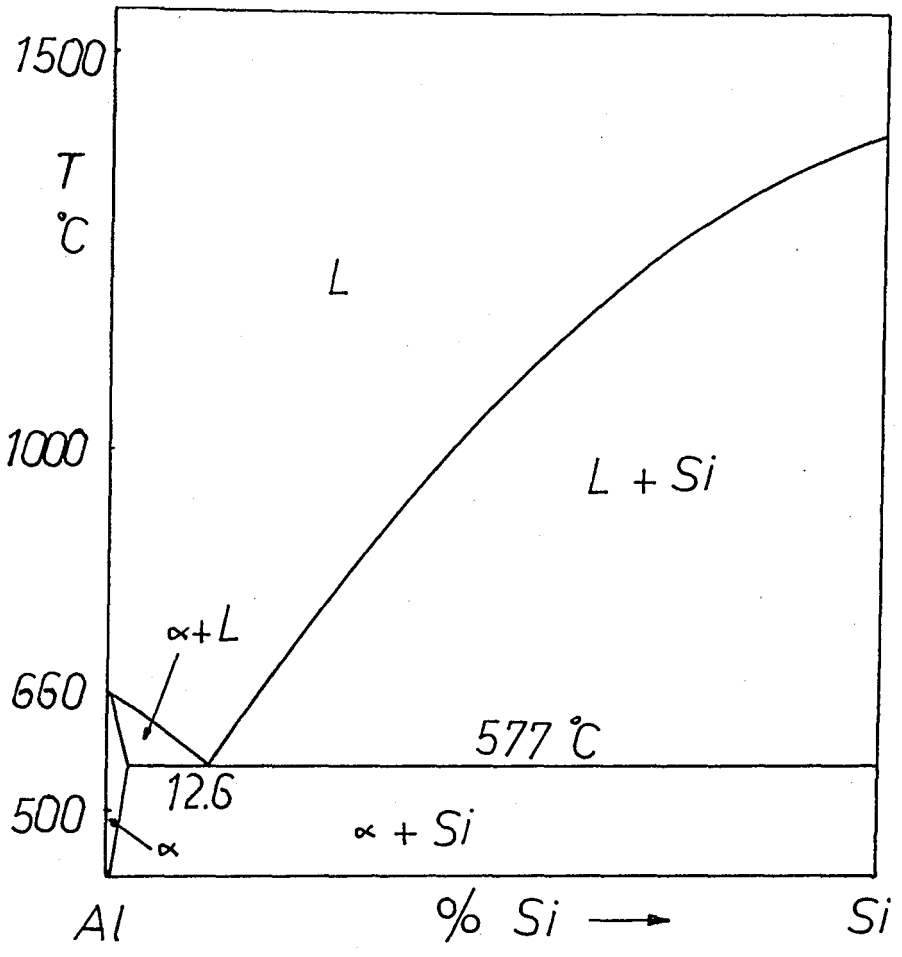

Figure 15 - The aluminum-silicon phase diagram.

3.3.2 Growth

The growth rods, prepared as mentioned above, have been inserted into cylindrical graphite crucibles of 10 cm length and 4 mm inner diameter. A steel weight was attached to the bottom end of the crucible and the top end was connected to the pulley system and subsequently suspended into the vertical growth furnace. Independent control of the resistance heaters enabled establishment of accurate temperature gradient, during experiments extending linearly throughout the hot zone

of growth furnace. The correction of which was also confirmed through other thermocouples leaded to the potensiometer. After a stabilized temperature gradient was achieved, motor was started and the growth rod descended with a predetermined rate.

3.3.3 Metallographic Examination

The resultant microstructures were then subjected to detailed investigation by standard metallographic techniques. Both longitudinal and transverse sections were taken, mounted and polished down to 500 grade emery paper. Final polishing was performed using diamond polishers. The microstructure was revealed by etching the polished surface with hydrofluoric acid solution (1 ml HF, 200 ml water). This reagent was swabbed for 15 seconds to the sample surface, washed and then blown dried with alcohol.

After all these processes, sectioned samples were ready to study under microscope. An Olympus microscope with unitron micrometer lenses was used for the measurement of interparticle spacing, λ. In quantitative microscopy, λ, essentially the mean particle center-to-center length, can be defined by,

$$\lambda = 1/N_L \tag{8}$$

Here, N_L is the number of particle interceptions per unit length of a random test line. Interparticle spacings were obtained by averaging at least 6 different measurements taken from each of seven regions as shown in Figure 17. Also photography was carried out by means of an Olympus camera attachment.

3.3.4 Mechanical Testing

Specimens were subjected to both tensile and vickers hardness tests. First, directionally solidified rods were machined down to 4.5 mm gage diameter and 20 mm gage length tensile test specimens, as illustrated in Figure 16. Then the surfaces were carefully hand polished in order to eliminate any surface defects introduced by machining. The tensile tests were performed on a MTS testing machine at room temperature. Vickers hardness measurements were taken employing 5 kg load. Vickers hardness number defined by,

$$VHN = \frac{1.854F}{L^2} \tag{9}$$

where, F is the applied load and L is the average value of the diagonals of indentation.

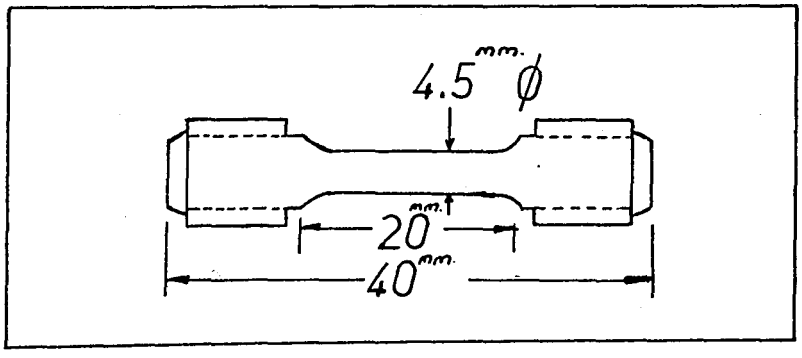

Figure 16 - Schematic view of the tensile specimen.

VI. RESULTS AND DISCUSSION

4.1 MICROSTRUCTURAL EXAMINATION

4.1.1 Introduction

Data regarding the silicon morphology and interparticle spacing have been collected from the microanalysis of seven different regions of each specimen. These are illustrated in Figure 17.

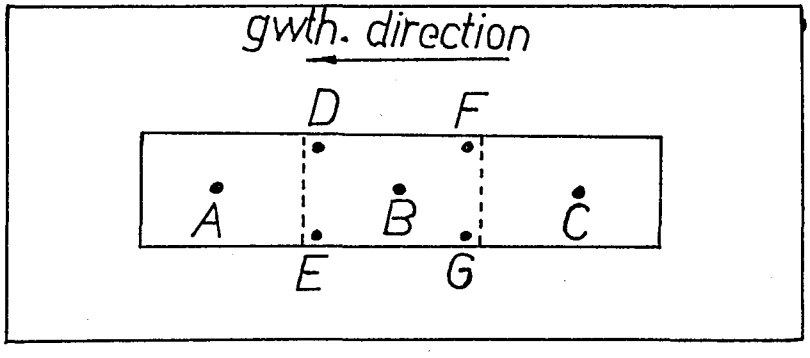

Figure 17 - Schematic view of the sections of micrographs.

Results of the interparticle spacing measurements were listed in Tables 2 to 8. Typical of the micrographs illustrating the variation of microstructure with respect to antimony concentration and growth parameters have been presented in Figures 18 and 19. Data

in tables 2 to 7 have been summarized in the form of λ versus G_L and λ versus R plots for both unmodified and antimony treated Al-Si eutectic alloys are graphically presented in Figures 21 to 29 in log-log scale; when doing this, attention was paid to a particular central location of the grown samples, such as point B in Figure 17. From the work, interparticle spacing, λ, has also been plotted against the solidification parameter, $G_L R$ (termed as the cooling rate) in Figures 33 to 38 in log-log scale.

Results of the mechanical tests were listed in Table 9, where both the strength and Vickers hardness values were outlined. Data in Table 9 have been graphically presented in the form of UTS versus R, YS versus $\lambda^{-\frac{1}{2}}$ and R in Figures from 39 to 43. Also UTS and YS versus antimony concentration plots were summarized in Figures 44 and 45 respectively, with different growth rates.

4.1.2 Characteristics of Unmodified Al-Si Eutectic Alloys

In the present work, specimens were solidified with growth rates in the range from 0.002 cm/sec to 0.05 cm/sec and with temperature gradients varying from 10^{o}C/cm to 40^{o}C/cm. Therefore, the growth conditions fall into the region C of the classical G_L versus R plot of Day [11] as already presented in Figure 7. Actually, much of the conventional casting conditions fall into this region, accordingly present unidirectional growth experiments may also be helpful in predicting the possible effect of antimony in normal casting practice. The structural characteristics of the sample grown in region C is

such that, irregular flake-type morphology of silicon particles predominates, which is suggested to form by the growth of silicon phase as a stack of twins (1).

4.1.2.1 Morphological Appearance of Al-Si Unmodified Structure

Typical of the unidirectionally grown Al-Si eutectics are seen in Figures 18 and 19a where, massive crystals of the two phases are obvious. In addition to this, as clearly demonstrated in Figure 20a,b, dendritic morphology of primary α-Al is part of the structure irrespective of the growth conditions employed. However, comparative microexaminations have shown that fraction of primary α-Al increases as growth rate increases, in full agreement with the observations of Steen and Hellawell [12] as seen in Figure 8. Unfortunately, the work could not be extended in order to investigate the orientation relationship between Al and Si particles. But it is known from a past work [11] that, there exists no consistent orientation relationship between these phases.

4.1.2.2 Effect of Solidification Parameters upon Unmodified Al-Si Eutectic Structure

Following deductions were apparently possible from Table 2. For a particular growth condition, interparticle spacing, λ, showed some amount of variation between different regions of each sample. However, such variations were not consistent and its determination was time consuming, therefore the measurements of the effect of

temperature gradient, G_L, and growth rate, R, upon the interparticle spacing, λ, were confined to collect the measurement data from region B. Particular attention upon the λ measurements shows that, this parameter proves variations with both the temperature gradient and the growth rate. However, in much of the cases, variations with G_L was reasonably small, not exceeding 10% for the change of G_L for $40^oC/cm$ to $10^oC/cm$. Graphical presentation of λ versus G_L for different growth conditions is given in Figure 21. Obviously λ varies linearly with G_L, irrespective of the growth rate. It is noted that the slope of such variations does not exceed 0.07. It is also seen that G_L was more effective at higher values of R.

The equations of the λ versus G_L plots can be written as,

$$\log \lambda = \log C_1 + m_1 \log G_L \qquad \text{for } R_1$$
$$\log \lambda = \log C_2 + m_2 \log G_L \qquad \text{for } R_2$$
$$\log \lambda = \log C_3 + m_3 \log G_L \qquad \text{for } R_3$$

The slopes of the lines are very small and if they are neglected,

$$\log \lambda = \log C$$

can be written for a given R. Then log C versus growth rate, log R, plot can also be drawn, as seen in Figure 29. Obviously, this allows the following equation to be valid.

$$\log C = \log K + n \log R$$

where the slope n appeared to be -0.30. That means

$$\lambda \propto R^{-0.30} \qquad \text{since,} \qquad \log \lambda = \log C$$

relation was assumed. On the other hand, effect of R upon λ, in all cases was remarkable. λ measurements have shown up to 40% decrease in every region of the samples with the change of R from 0.002 cm/sec to 0.05 cm/sec λ versus R plots at different G_L values, again confined to the region B examinations, are presented in Figure 22. Clearly, plots resulted in a linear relationship, the slope varying around -0.30. Moreover, plots obtained at different G_L values nearly coincide, thus it is possible to conclude that λ vs R variation is independent of G_L within the experimental range selected for the present work.

Variation of λ with R can be expressed by an equation,

$$\log \lambda = \log C + n \log R$$

or

$$\lambda \propto R^n$$

where the average value of n is -0.30 for unmodified Al-Si structure.

Day [11] has found $\lambda \propto R^{-0.46}$ relationship existed in the unidirectionally grown Al-Si eutectic alloys. Others have found the $\lambda \propto R^{-0.41}$ relation [20]. Obviously there is considerable difference between the growth rate exponent, n, measured in this work and those found in the past investigations, which can be averaged to the value of -0.43. Discrepancy between the results can well be accounted by the differences in the experimental conditions. It is understood that, Day's [11] results were taken with the temperature gradients that mostly fall into the range from 10^{o}C/cm to 100^{o}C/cm, whereas, Yılmaz [20]

has carried out his experiments with gradients around $100^{o}C/cm$ or more. Therefore, differences of the rate exponent measurements can possibly be the result of the gradients employed, higher gradients causing higher values of n. At this stage, one should also consider the role of different measurement methods employed in various works. There exists no theoretical evaluation for the validity of the $\lambda \propto R^{n}$ relationship observed in the present analysis. Hunt and Jackson [5], in their theoretical work, estimated n as to be -0.5 for normal eutectic structures. But there is no way of applying their analysis to anomalous Al-Si eutectic solidification, because of the requirements of extra kinetic problems for silicon growth.

Attempts have also been made to search for a correlation between λ and another unidirectional solidification parameter, $G_L R$. The results have been obtained in graphical form in Figure 33. Data points apparently accumulated around a straight line and can be expressed by an equation of the form,

$$\log \lambda = \log K + S \log(G_L R)$$

or

$$\lambda \propto (G_L R)^{S} \qquad \text{where} \quad S = -0.15 \text{ in this work.}$$

4.1.3 Characteristics of Antimony Modified Al-Si Eutectic Alloys

4.1.3.1 Effect of Antimony upon Morphology of Al-Si Eutectic Structure

In antimony modified Al-Si structure, silicon crystal sizes were reduced, as well as the spacings between them, as in Figure 18 b.

Also, modification leaded to more frequent overgrowth by the aluminum phase, which appeared as primary aluminum dendrites, mostly aligned in the growth direction as in Figure 20 c, d, e and f. It was found that their fractions increased with increasing growth rate and antimony concentration. At higher concentrations of antimony, the structure became coarser in the sense that silicon particles were again enlarged and interparticle spacings were increased as shown in Figure 18 b, c, d, e, f. The antimony containing phase AlSb was determined by optical microscopy as dark faceted particles in Figure 18 g. This was also observed by Yaneva [17]. But in the case of sodium and strontium modifications, flake morphology transformed into a fibrous form [1,20]. At high concentration levels, some overmodification bands were observed [1].

4.1.3.2 Effect of Solidification Parameters upon Sb-Modified Al-Si Eutectic Structure

In the present investigation, attempts have been made to modify the Al-Si eutectic structure by antimony treatment using 0.1 to 2 wt% Sb with varying G_L and R. The results regarding the dependence of λ upon G_L, in presence of different Sb additions, have been compared with the data collected from unmodified experiments in Figures from 23 to 25. Clearly, for a constant growth rate, R, antimony addition has produced much finer interparticle spacings when compared with the unmodified structure. On the other hand, log λ versus log G_L diagrams are antimony content dependent.

When the interparticle spacing is plotted against the antimony content at a given temperature gradient and growth rate as seen in

Figures from 30 to 32, antimony effect tend to reach an optimum level in modifying the structure at a weight fraction of 0.1% in all combinations of G_L and R.

Two aspects can be deduced;

i. In presence of antimony, λ increases consistently as the antimony content varies from 0.1 wt% to 2 wt%

ii. The slope, i.e. the gradient component, m, tend to increase with increasing antimony fraction at higher growth rates, but remains unaffected at lower values of this parameter.

The logarithmic relationship between λ and R, in presence of antimony, was also found linear, as given in Figures from 26 to 28. Antimony addition results in a remarkable decrease in the interparticle spacing at a constant temperature gradient. Furthermore, effect of antimony decreases with increasing antimony fractions. It is apparent that the rate exponent is dependent upon the antimony content and its value becomes less negative with decreasing antimony percentage. In fact such variations may be around 16% for antimony content varying in the range from 0.1 wt% to 2 wt%.

In the λ versus cooling rate $G_L R$, plots, it was observed that at every antimony concentrations a linear relation was found to be valid and again the cooling rate exponent, S, is antimony content dependent. This exponent increases as the percentage of antimony varies from 0.1 to 2.

It is implicit in the foregoing presentation that antimony is the most effective at a fraction 0.1 wt% for every value of G_L and R.

This observation is, in fact, in full agreement with the findings of Yaneva [17], which is the only data available in the literature. The effect of antimony in modifying the Al-Si structure remains a problem to be solved. It is apparent that the number of Si particle is much more after modification which means that more nucleation must have occurred in the modified structure. And it is known that the more undercooling causes the greater nucleation rate. Thus, modification can be associated to an undercooling rise at the solidification front. But there are two possibilities [26];

i. Extra nucleation may be necessary, because the growing particles of silicon are prevented from growing to a large size by high concentrations of the modifying agent ahead of the solid-liquid interface. If the particles can not grow, fresh nucleation must occur since the solidification is to continue.

ii. Nucleation of all the silicon particles is retarded by the modifying agent and this results larger amount of undercooling, which is turn creates nucleation to produce smaller silicon particles.

It is known from the previous works [1,14,19] that sodium and strontium modifications owe their origin to the definite undercooling rising at the growth interface. Flood and Hunt [1] proposed that sodium prevents nucleation occurring ahead of the eutectic growth front and this leaded a larger undercooling. Therefore, the mechanism of antimony could well be explained in a similar manner. If these were

really what has happened, antimony prevents silicon crystals to grow to large sizes by high concentration of the antimony existing at the solid-liquid interface. Thus this causes larger amounts of undercooling and greater nucleation rate of the silicon particles. Yaneva [17] claimed that, antimony addition retards the growth of silicon crystals and causing greater interface undercooling, eventhough they have presented no undercooling data. The diminish in refinement at concentrations higher than 0.1 wt% can be explained due to the formation of a new solid phase between aluminum and antimony [AlSb], which causes a strong reduction of antimony from the growth front and decreases the effect of modification.

4.2 MECHANICAL PROPERTIES OF Al-Si EUTECTIC ALLOYS

4.2.1 Mechanical Properties of Unmodified Structure

The tensile strength of unmodified chill-cast Al-Si eutectic alloys is normally around 19 kg/mm^2 [12,14]. In directionally grown samples of the same alloy, tensile strength has been measured as 12 kg/mm^2 for growth rates about $8x10^{-3}$ cm/sec [12].

The mechanical properties of unmodified unidirectionally grown Al-Si eutectic alloys of the present work were outlined in Table 9, where the variation of both the tensile strength and hardness with growth conditions can be followed. It is seen clearly that, for a constant gradient at the growth interface, the tensile strength increases from 12.64 kg/mm^2 to 15.47 kg/mm^2 as the growth rate increased from 0.002 cm/sec to 0.05 cm/sec. In fact, UTS vs R

plot as seen in Figure 39, is almost linear. Therefore the results regarding numerical values are comparable with those obtained by Steen and Hellawell [12].

The yield strength of the materials has been defined by 0.2 pct elongation offset point and this parameter has proved a curved variation with the growth rate, R, as presented in Figure 40. Also it was claimed that [22] Hall-Petch type relationship exists between yield strength and interparticle spacing in normal structures. Validity of this proposal has been tested by a plot of YS vs $\lambda^{-\frac{1}{2}}$ as presented in Figure 41. Apparently, the relationship is non-linear. Also, recalling that $\lambda \propto R^{-0.30}$ relation holds, another method of testing the validity of Hall-Petch relation is to plot YS vs $R^{1/6}$. This has been done and the result is given in Figure 42. The relationship is again a curved one. Thus, it is possible to question the validity of Hall-Petch relation in works of this kind.

It is also known that decreasing interparticle spacing increases hardness of materials. Vickers hardness numbers were found to increase about 23% when the growth rate increased from 0.002 cm/sec to 0.05 cm/sec. Temperature gradient was observed to have no significant effect on UTS, YS and VHN, which is consistent with microstructural analysis.

4.2.2 Mechanical Properties of Sb-Modified Al-Si Eutectic Alloys

The tensile strength of antimony-modified castings was found to be about 20 kg/mm^2 and has been said to increase by heat treatment

to about 28 kg/mm^2[2]. In addition, tensile strength of sodium-modified chill-cast alloys was found to be around 22 kg/mm^2[14].

The mechanical properties of modified unidirectionally grown Al-Si eutectic alloys of the present work were tabulated in Table 9, where strength and hardness values with different growth conditions can be followed. It was found that tensile strength is 18.86 kg/mm^2 at a growth rate of $5x10^{-2}$ cm/sec. In UTS vs R plots, as seen in Figure 39, tensile strength increases with growth rate and curves tend to level out at higher values of growth rate. Obviously, the yield strength increases with growth rate in parallel with the variation between UTS and R, eventhough uncertainties arises in the measurement of 0.2 pct yield strength.

An interesting result is the effect of antimony content upon the UTS and YS. It is seen clearly from Figure 39 that, at a constant growth rate, the strength of the material decreases with the increase of antimony content from 0.1 to 0.5 wt%. Thus a better way of evaluating the effect of antimony content was to plot UTS vs C_{Sb}, as given in Figures 44 and 45. Apparently, for a given growth rate, strength reaches a maximum at Sb additions around 0.1 wt% and then decreases gradually as the Sb content increases. It is seen that, in Figure 30, λ also reached a minimum at 0.1 wt% antimony. Therefore, it is concluded that strength of Al-Si alloy system is determined by the variation in λ to greater extend that the solute solution strengthening that could possibly arise from antimony additions. Also, as noted originally by Pacz [13], cracks propagate through the flaky form of silicon. Cracks spread easily because the cleavage plane of

silicon is {111}, which often is the plane of faceted flakes.

In modified structure, Vickers hardness values reach a maximum at 0.1 wt% Sb and decrease gradually as Sb concentration increases.

4.3 OVERALL DISCUSSION

In the present work, the structural modification features of Al-Si eutectic alloys with antimony treatment were investigated. The growth conditions used in the experiments fall into the region C in Figure 7. Many conventional casting conditions also fall into this region, so the present work is useful in predicting the structural modification of normal castings with antimony treatment. It was observed that the structure of unmodified Al-Si eutectic consists of massive crystals of silicon phase and primary α-Al dendrites. The growth parameters effect the structure such that, temperature gradient, G_L, does not have an important effect, not exceeding 10% for a change of G_L from $40^oC/cm$ to $10^oC/cm$, whereas the effect of growth rate is remarkable. Almost in all cases, 40% decrease in interparticle spacing have been observed with the change of R from 0.002 to 0.05 cm/sec. In λ versus R plots a relation of the form $\lambda \propto R^{-0.30}$ was found and discrepancy with other works were attributed to the differences in the experimental conditions used. Besides a combined effect of growth rate and temperature gradient which is called the cooling rate, $G_L R$, have been analysed and found a linear relationship exists between interparticle spacing and cooling rate. The effect of antimony upon the structure causes a decrease in silicon particle size and interparticle spacings. Also dendrite of α-Al increases with antimony

additions. In the antimony treated alloys, the interparticle spacing versus temperature gradient diagrams were found antimony content dependent. The relationship between λ and R was found to be linear and λ decreases remarkably as the growth rate increases. Also the cooling rate, $G_L R$, varies linearly with interparticle spacing in the modified alloys. It was observed that antimony effect reaches a maximum at 0.1 wt% for every value of G_L and R and the structure becomes coarser at higher concentrations. This behaviour can be attributed to that antimony addition prevents the silicon crystals to grow to large sizes by high concentration of the antimony at the solidification front. Thus, this causes an increase in undercooling at the growth interface and greater nucleation rate of silicon crystals which is responsible to much finer spacings observed in the modified structure. But, in order to prove the validity of this proposal, undercooling analysis has to be carried out in future works. The effect reduces at higher concentrations of antimony. This is due to the formation of AlSb phase, which causes a strong reduction of the antimony from the solid-liquid interface, causing a decrease in refinement of the structure.

The mechanical tests show that, UTS varies almost linearly with growth rate whereas variation of YS with R is a curved one in unmodified structure. In the case of modified structure, UTS and YS increase with growth rate and curves level out at higher values of growth rate. Besides, it was found that both UTS and YS reach a maximum at 0.1 wt% of antimony and decrease at higher values of antimony concentrations in agreement with the microstructural analysis.

Vickers hardness values were found maximum at 0.1 wt% of antimony and decreased gradually at higher additions of antimony. Also, it was observed that temperature gradient in the range from $40^{o}C/cm$ to $10^{o}C/cm$ does not have a remarkable effect on mechanical properties.

V. CONCLUSION

1. It can be concluded that, antimony refines the Al-Si eutectic structure, preventing the growth of the silicon crystals to enlarge by the existence of high antimony concentration at the solid-liquid interface.

2. The effect of antimony upon interparticle spacing reaches a maximum at 0.1 wt% antimony and the effect decreases at higher concentrations.

3. Temperature gradient in the range from $10^{o}C/cm$ to $40^{o}C/cm$ does not have a significant effect upon the Al-Si eutectic structure.

4. Growth rate has a remarkable effect on interparticle spacing. Relations between λ and R are found as,

   $\lambda \propto R^{-0.30}$ for unmodified structure.

   $\lambda \propto R^{-0.08}$ for 0.1 wt% of antimony treatment.

   $\lambda \propto R^{-0.12}$ for 2 wt% of antimony treatment.

5. The variations of λ with cooling rate, $G_L R$ are,

   $\lambda \propto (G_L R)^{-0.15}$ for unmodified structure.

$\lambda \propto (G_L R)^{-0.06}$ for 0.1 wt% of antimony treatment.

$\lambda \propto (G_L R)^{-0.10}$ for 2 wt% of antimony treatment

6. In the unmodified structure, the UTS increases monotonically with increasing growth rate whereas the variation of YS with R is non-linear.

   In the modified structure both UTS and YS increases with R and curves level out at higher values of growth rate.

7. The UTS and YS reach a maximum at 0.1 wt% of antimony and decrease gradually at higher concentrations at all growth conditions.

8. Vickers hardness values increase with growth rate and reach a maximum at 0.1 wt% of antimony.

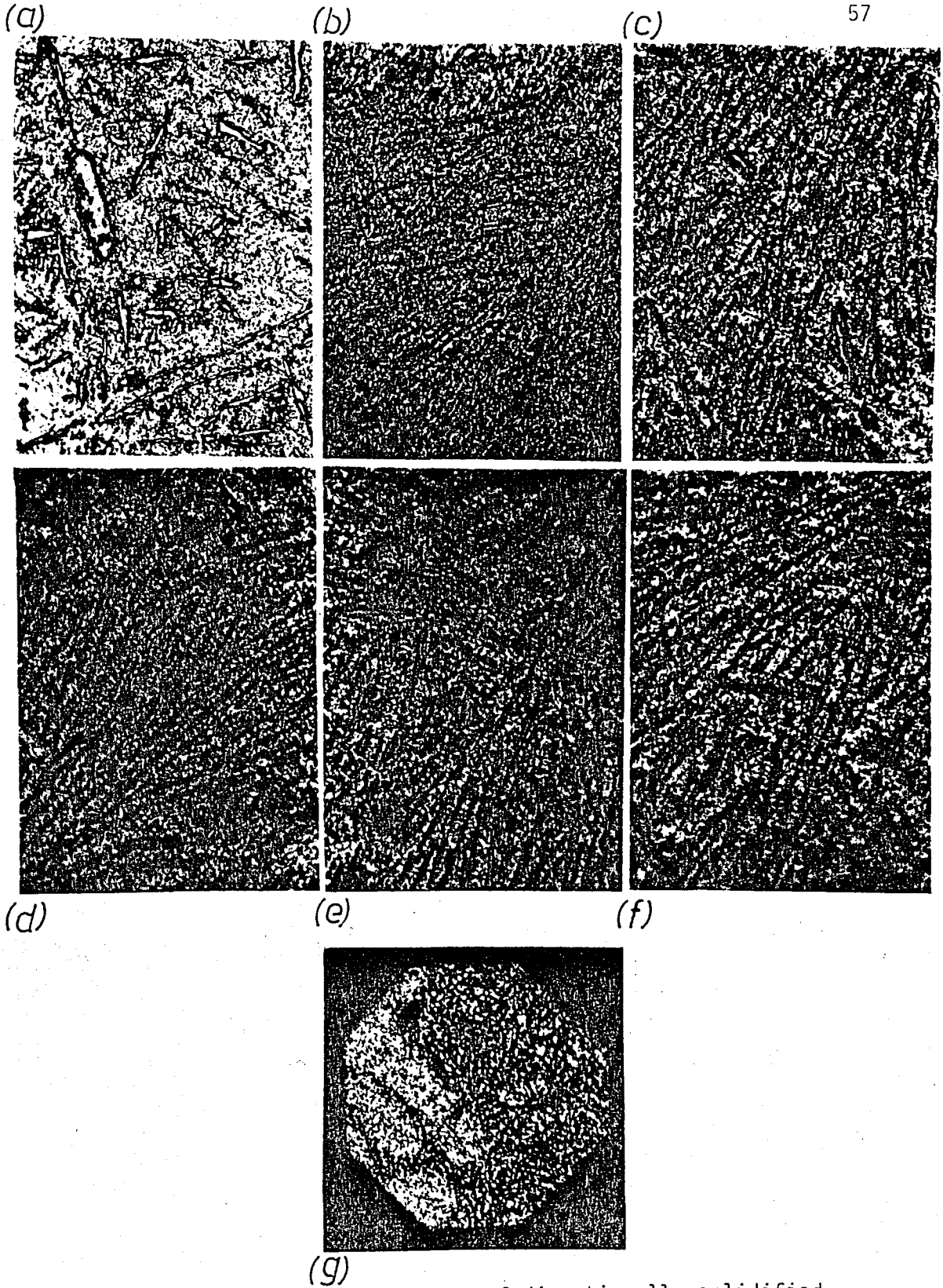

Figure 18 - Optical micrographs of directionally solidified Al-Si eutectic (x400)-longitudinal section. R = 0.002 cm/sec, G_L = 25°C/cm.

a) C_{Sb} = 0 wt% (b) C_{Sb} = 0.1 wt% (c) C_{Sb} = 0.2 wt%

d) C_{Sb} = 0.5 wt% (e) C_{Sb}= 1 wt% (f) C_{Sb} = 2 wt%

g) AlSb-phase particle

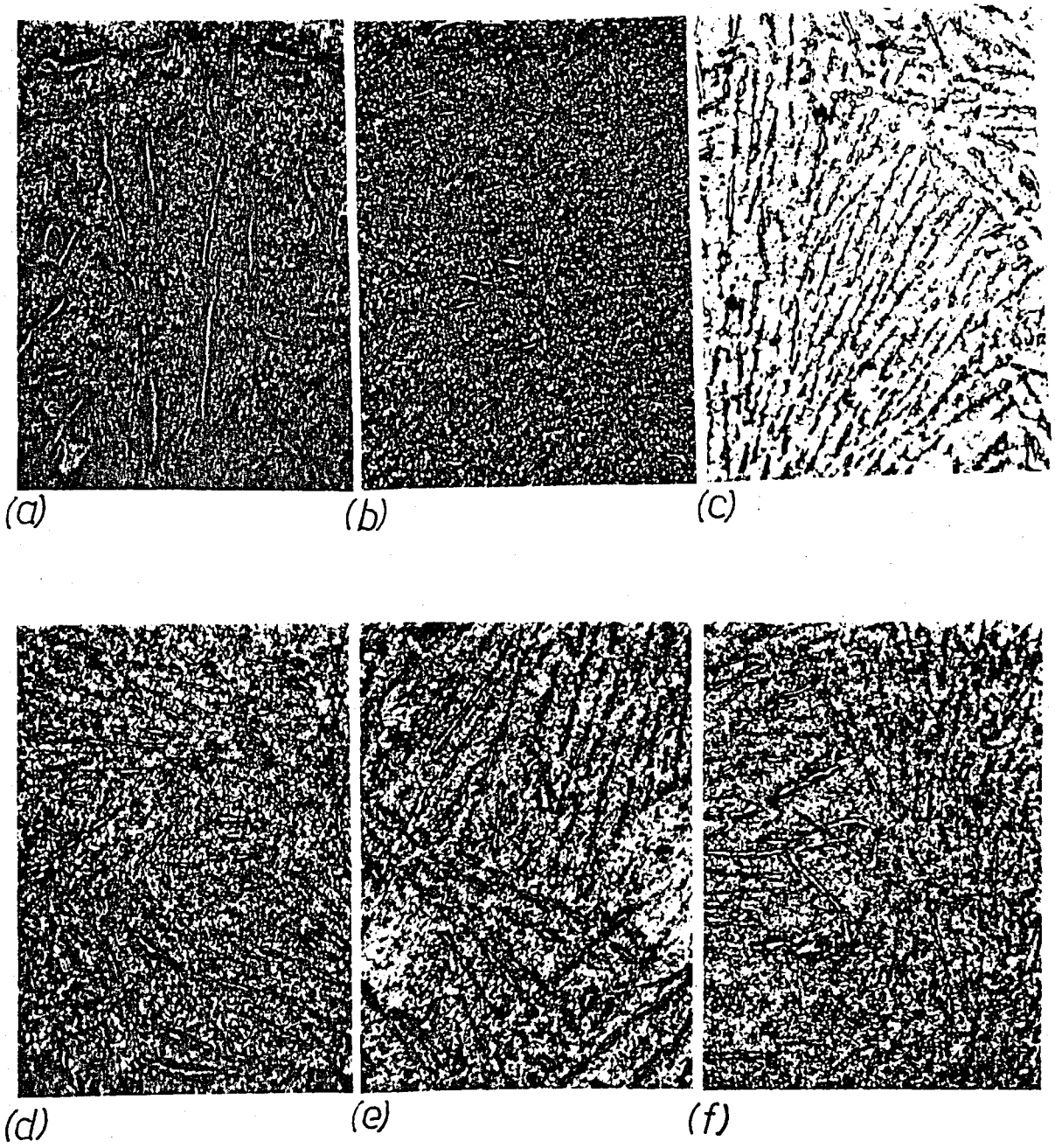

Figure 19 - Optical micrographs of directionally solidified Al-Si eutectic (x400)-transverse section. R = 0.002 cm/sec, G_L = 25°C/cm.

a) C_{Sb} = 0 wt% (b) C_{Sb} = 0.1 wt% (c) C_{Sb} = 0.2 wt%

d) C_{Sb} = 0.5 wt% (e) C_{Sb} = 1 wt% (f) C_{Sb} = 2 wt%

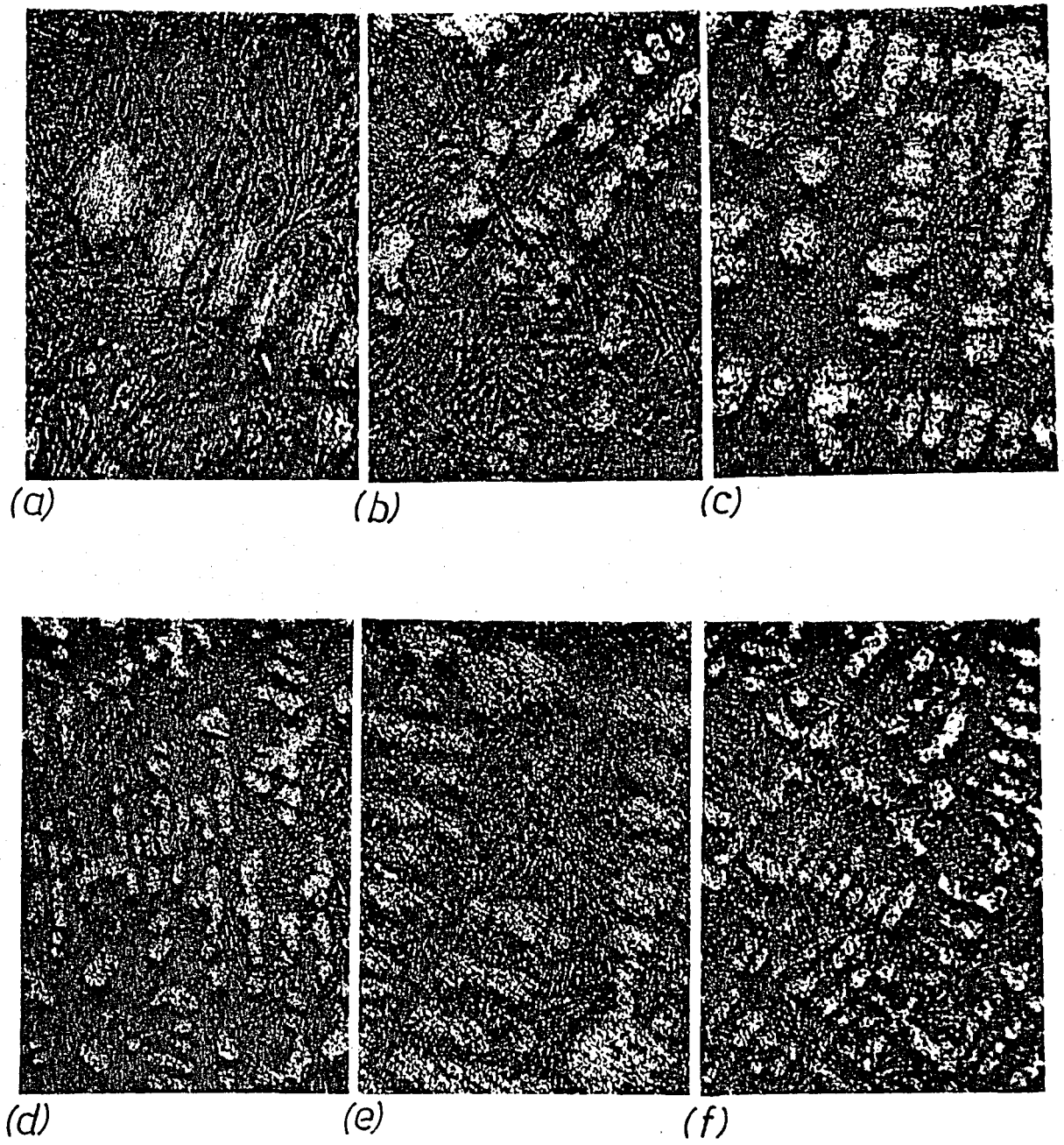

Figure 20 - Optical micrographs of primary-Al dendrites in directionally solidified Al-Si eutectic (x100)-longitudinal section. G_L = 25°C/cm

a) C_{Sb} = 0 wt% , R = 0.002 cm/sec (b) C_{Sb} = 0 wt% , R = 0.05 cm/sec

c) C_{Sb} = 0.1 wt%, R = 0.002 cm/sec (d) C_{Sb} = 0.1 wt%, R = 0.05 cm/sec

e) C_{Sb} = 1 wt% , R = 0.002 cm/sec (f) C_{Sb} = 1 wt% , R = 0.05 cm/sec

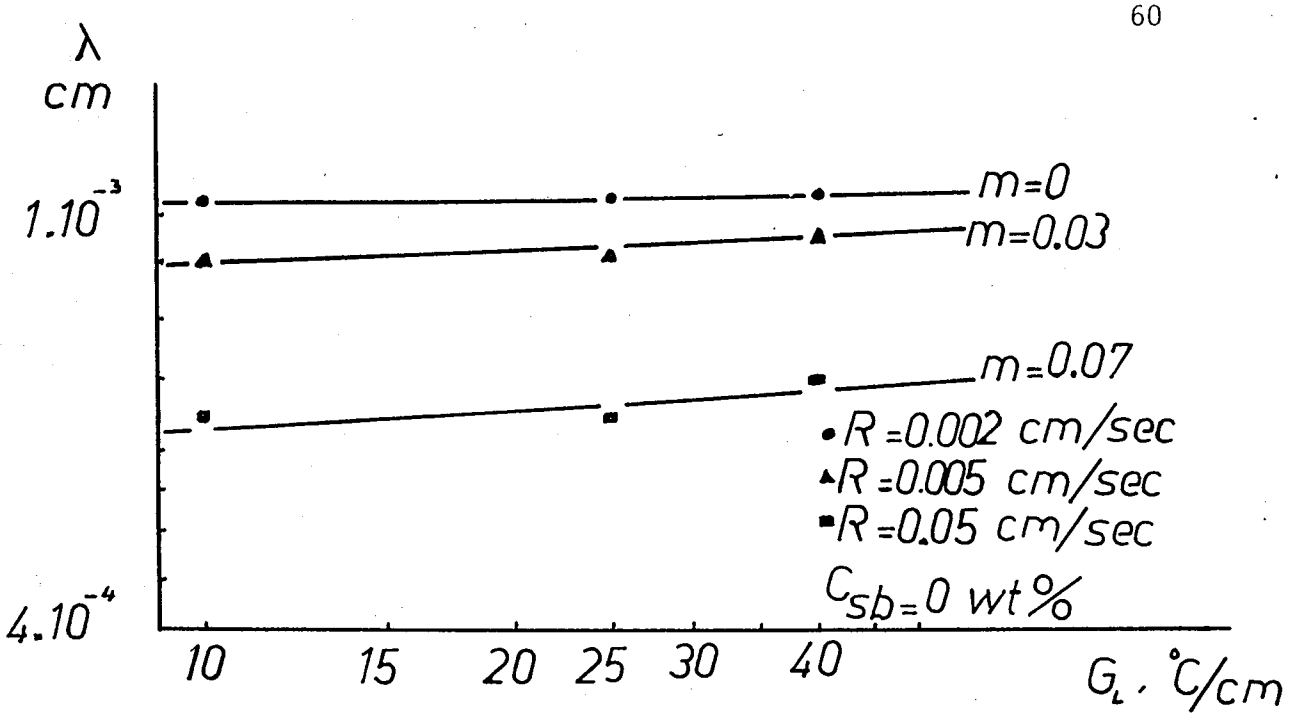

Figure 21 - Interparticle spacing versus temperature gradient plot.

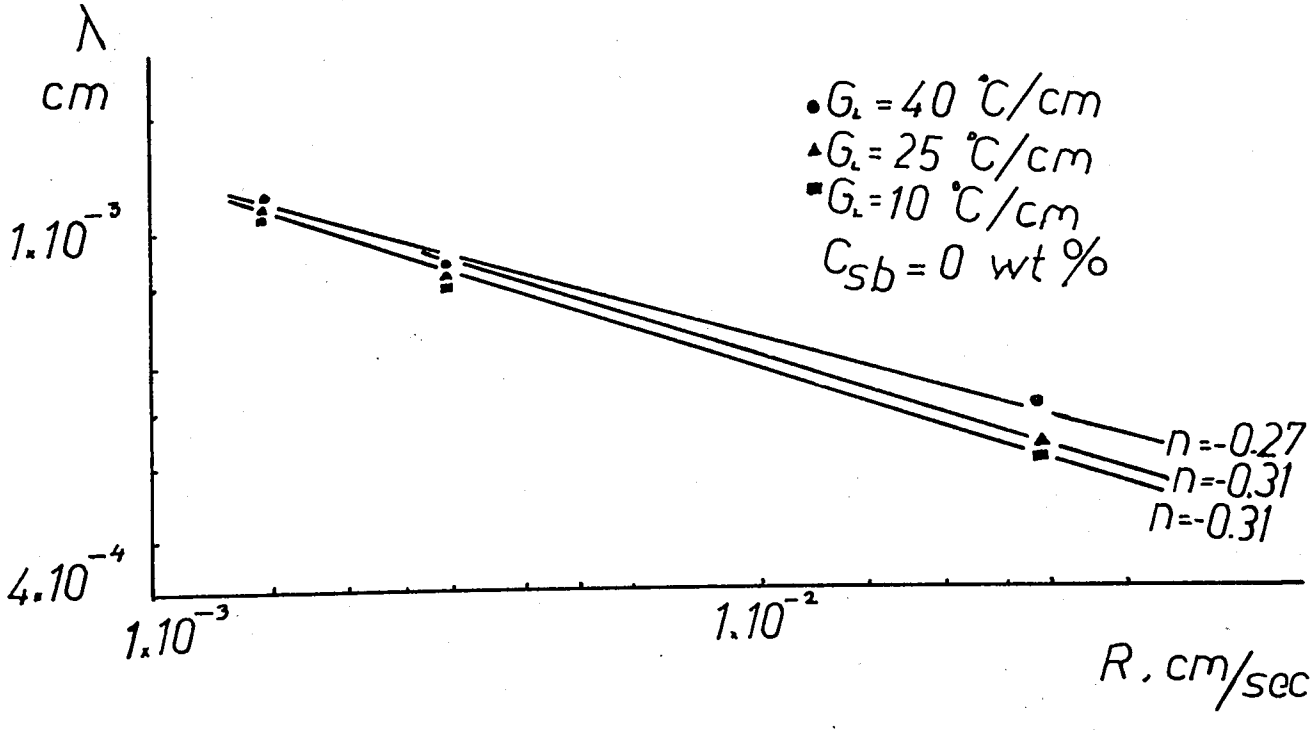

Figure 22 - Interparticle spacing versus growth rate plot.

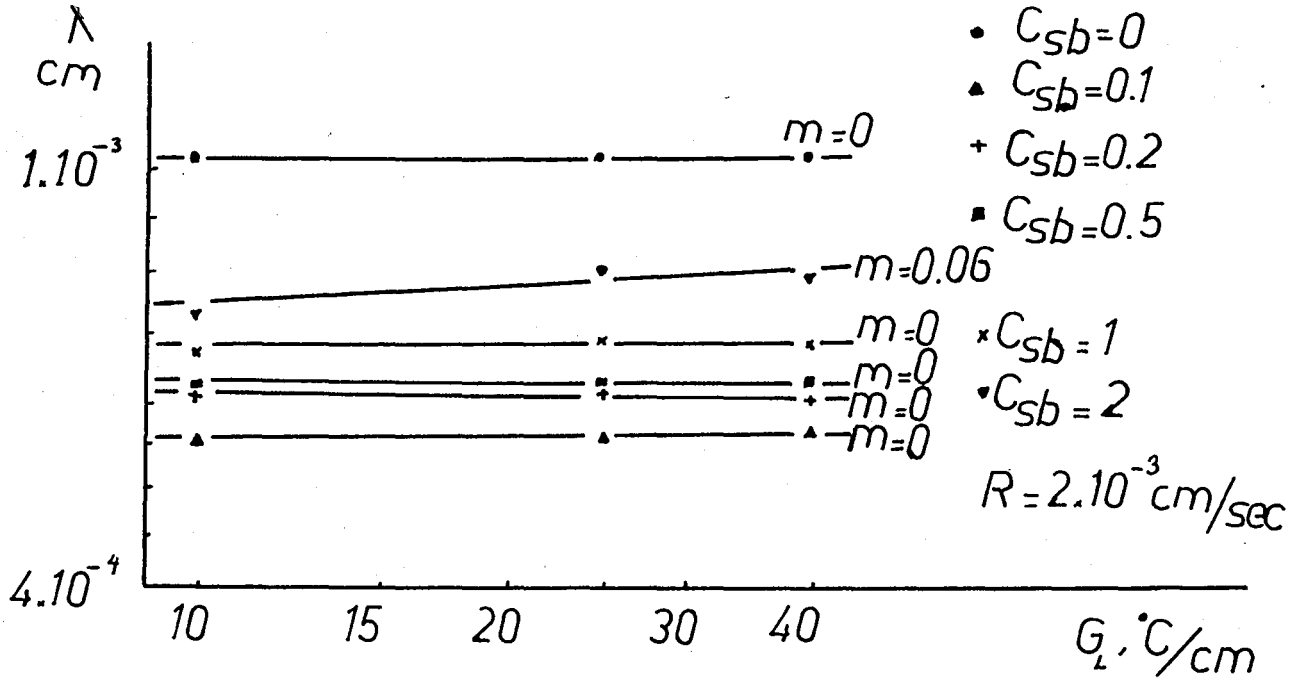

Figure 23 - Interparticle spacing versus temperature gradient plot.

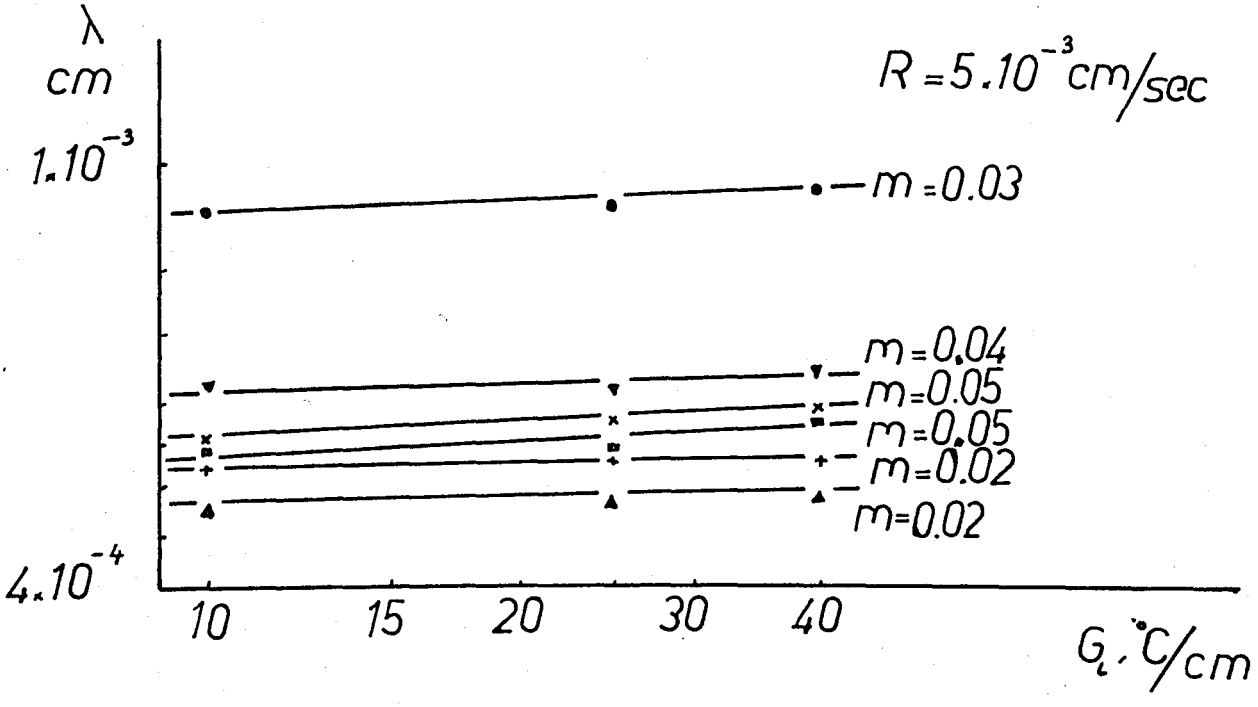

Figure 24 - Interparticle spacing versus temperature gradient plot.

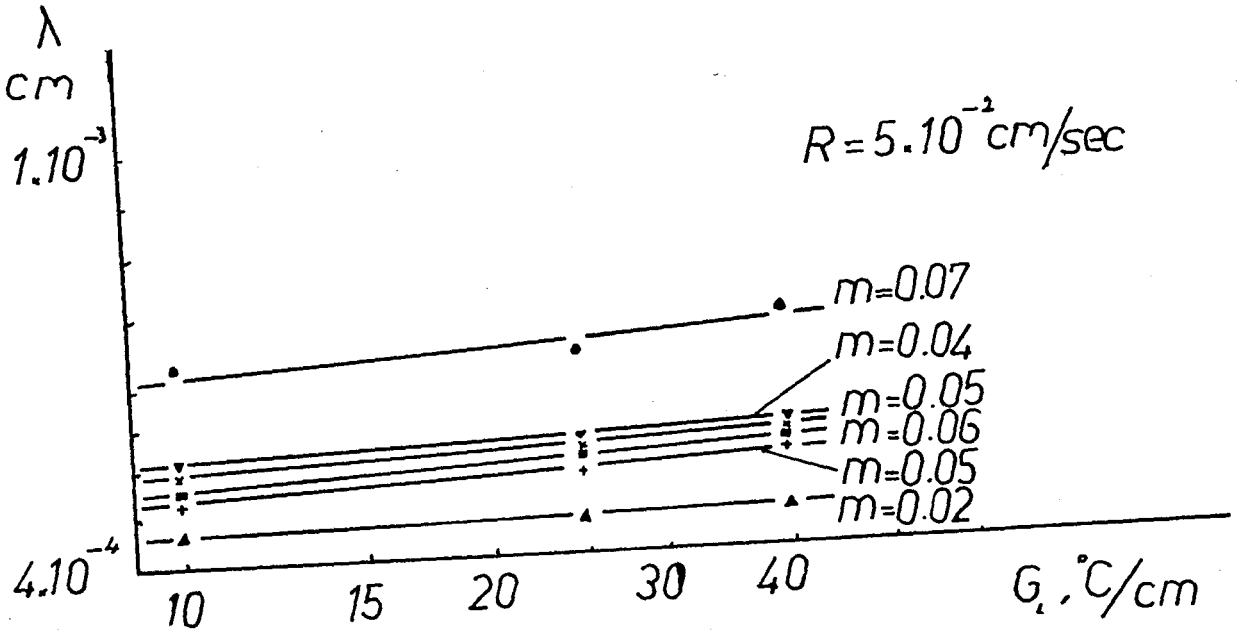

Figure 25 - Interparticle spacing versus temperature gradient plot.

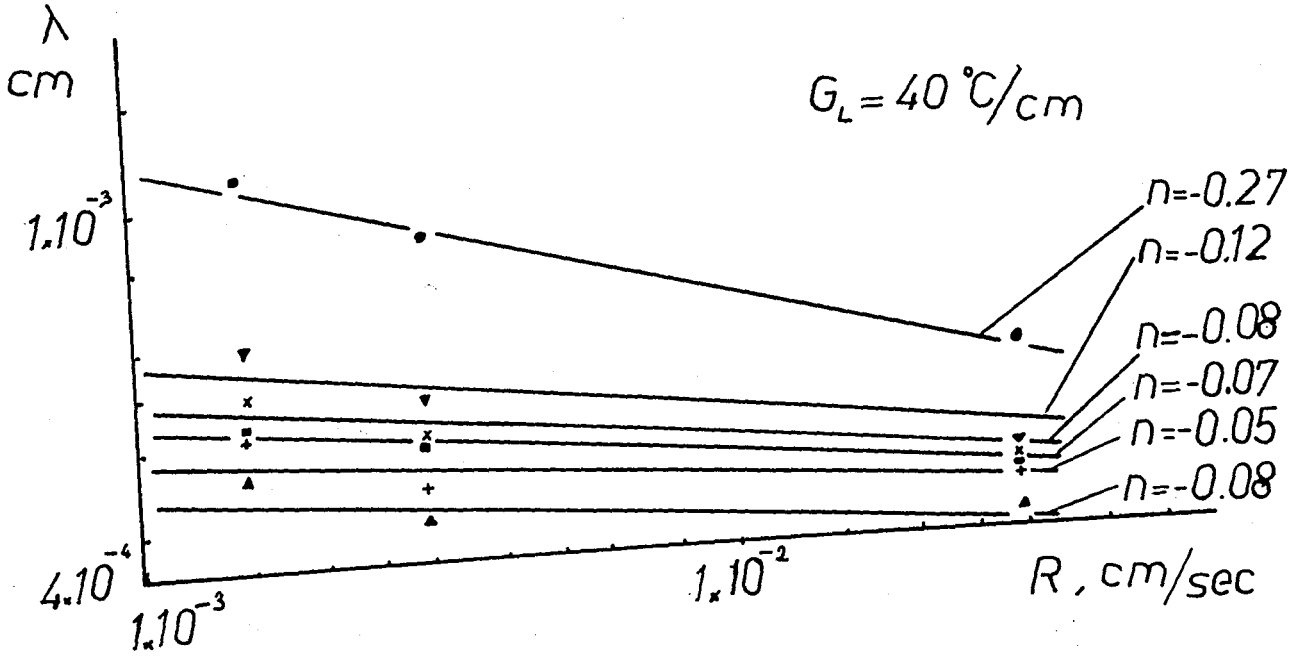

Figure 26 - Interparticle spacing versus growth rate plot.

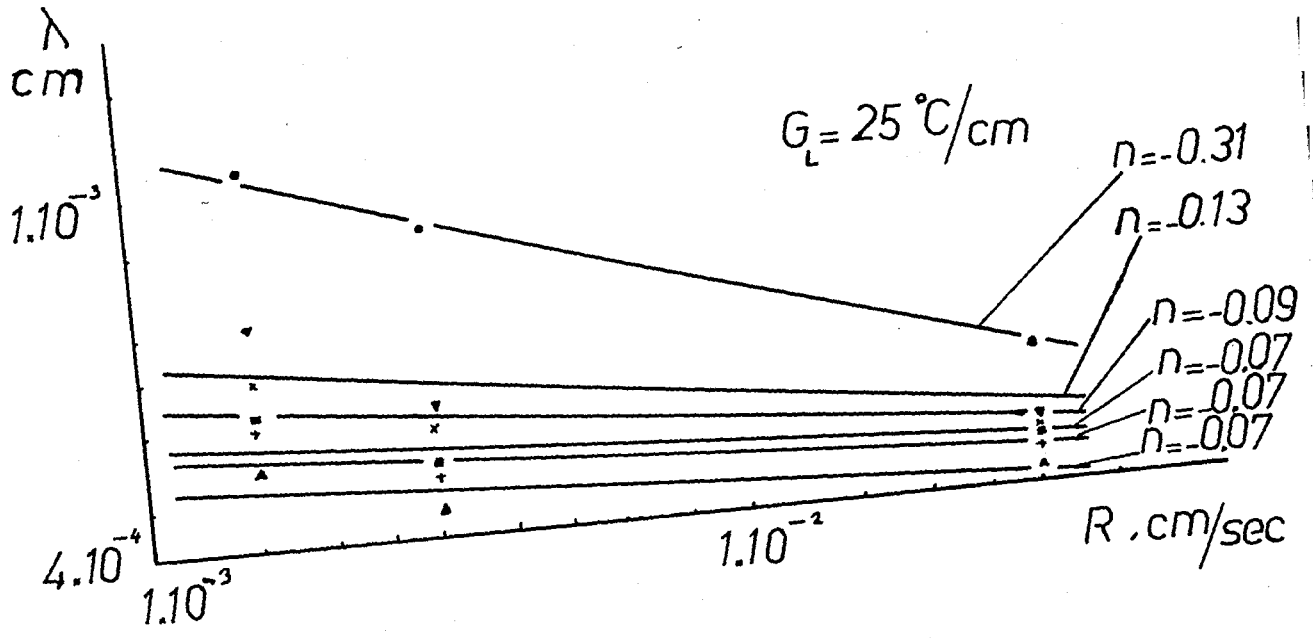

Figure 27 - Interparticle spacing versus growth rate plot.

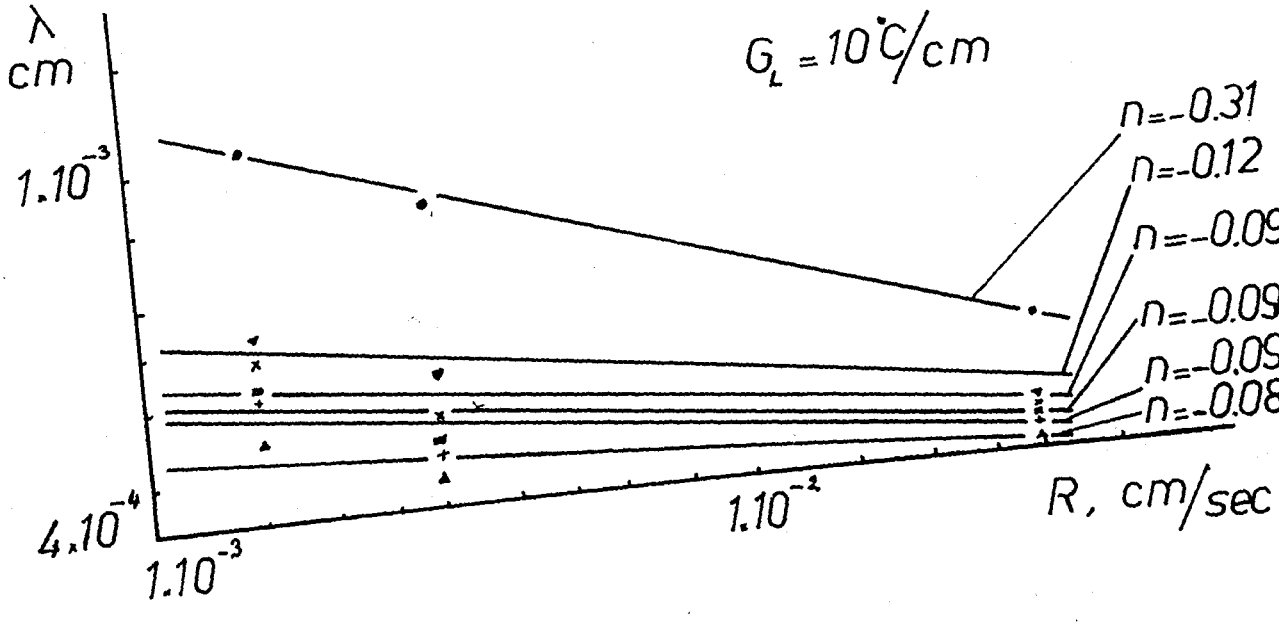

Figure 28 - Interparticle spacing versus growth rate plot.

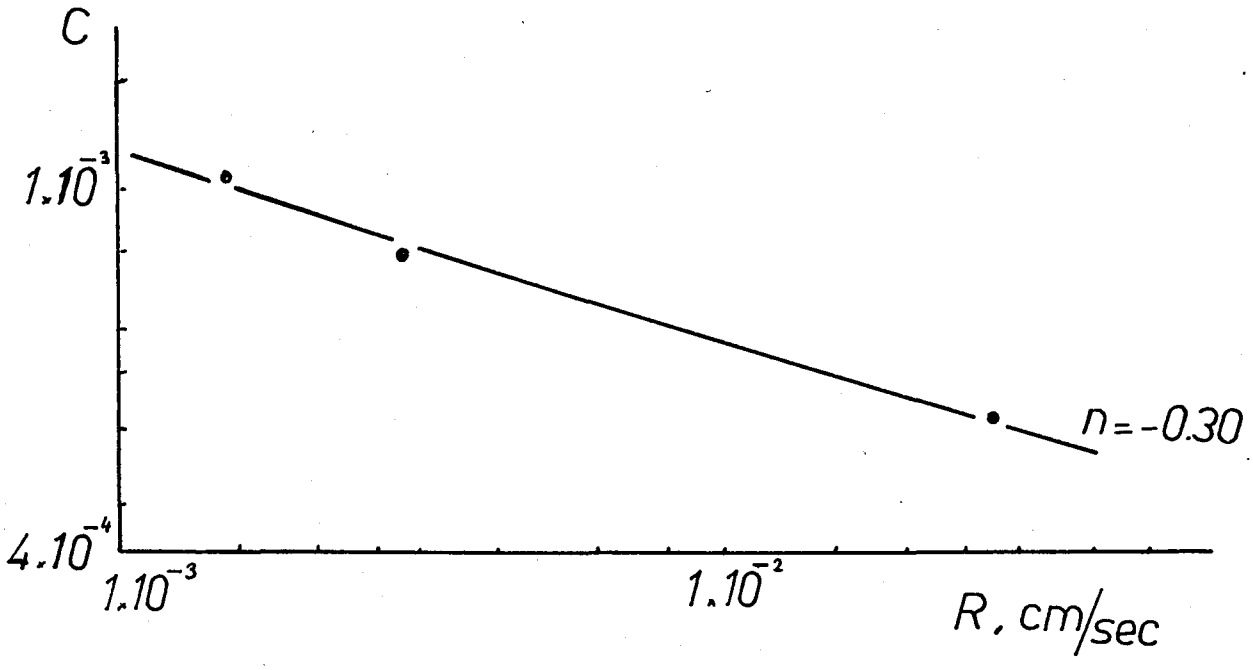

Figure 29 - Gradient intercept versus growth rate plot.

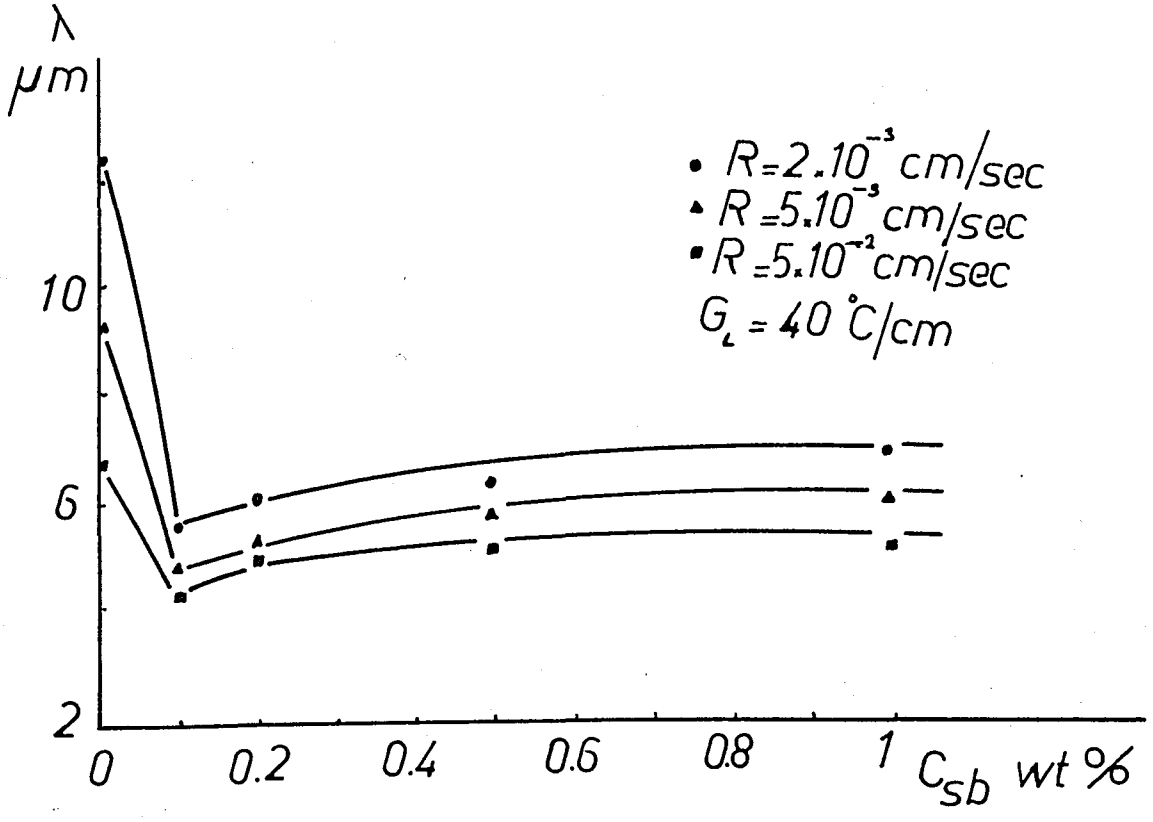

Figure 30 - Interparticle spacing versus antimony concentration plot.

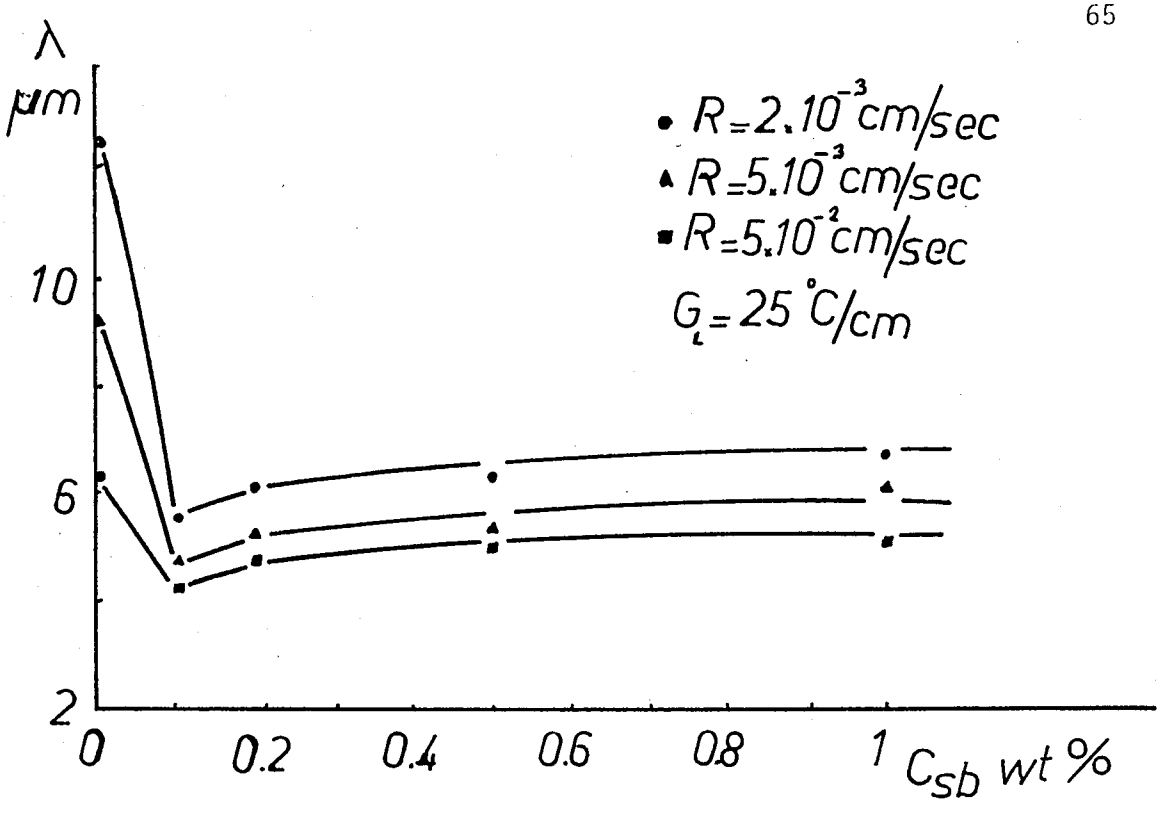

Figure 31 - Interparticle spacing versus antimony concentration plot.

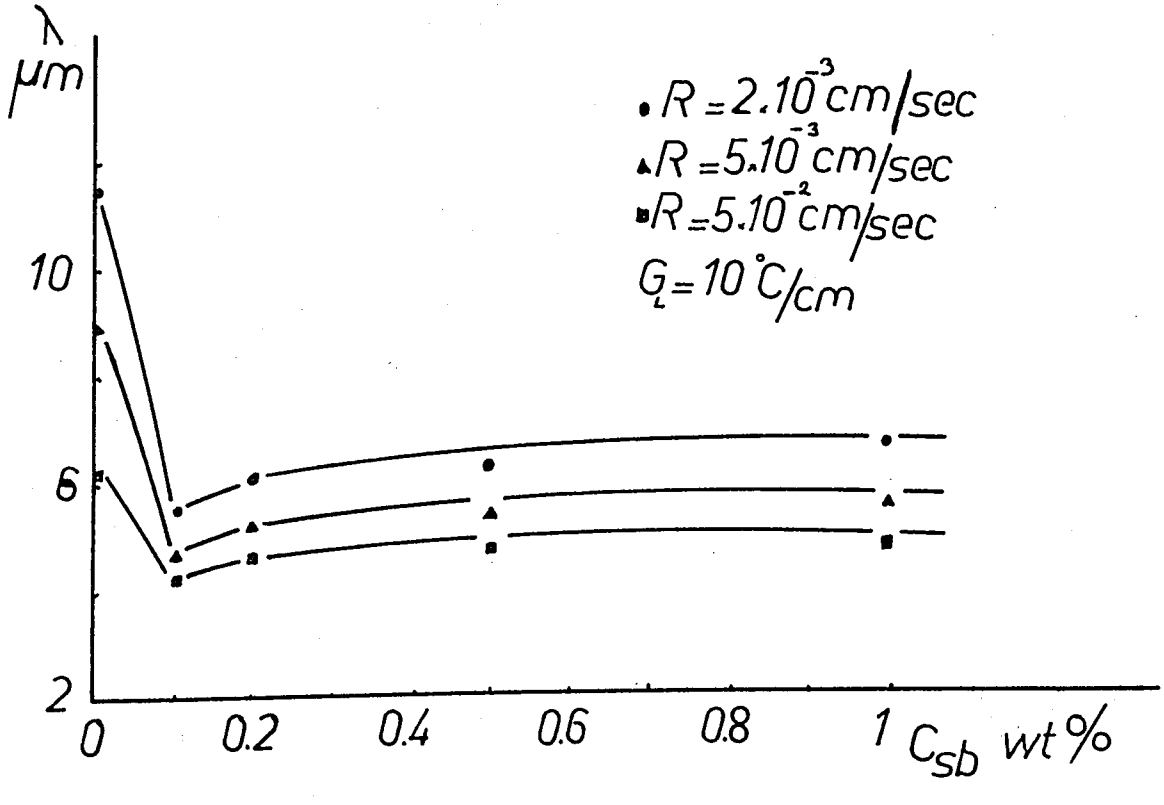

Figure 32 - Interparticle spacing versus antimony concentration plot.

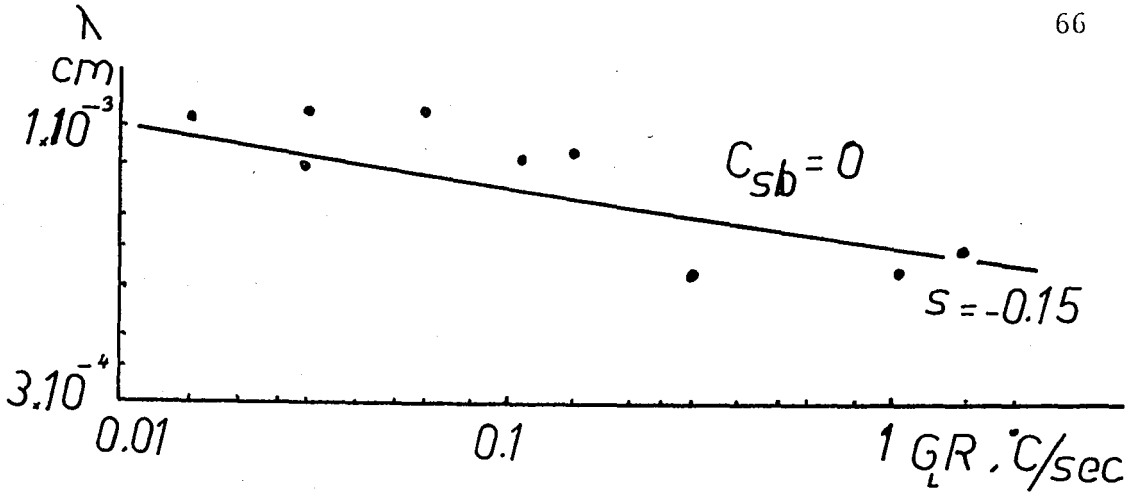

Figure 33 - Interparticle spacing versus cooling rate plot.

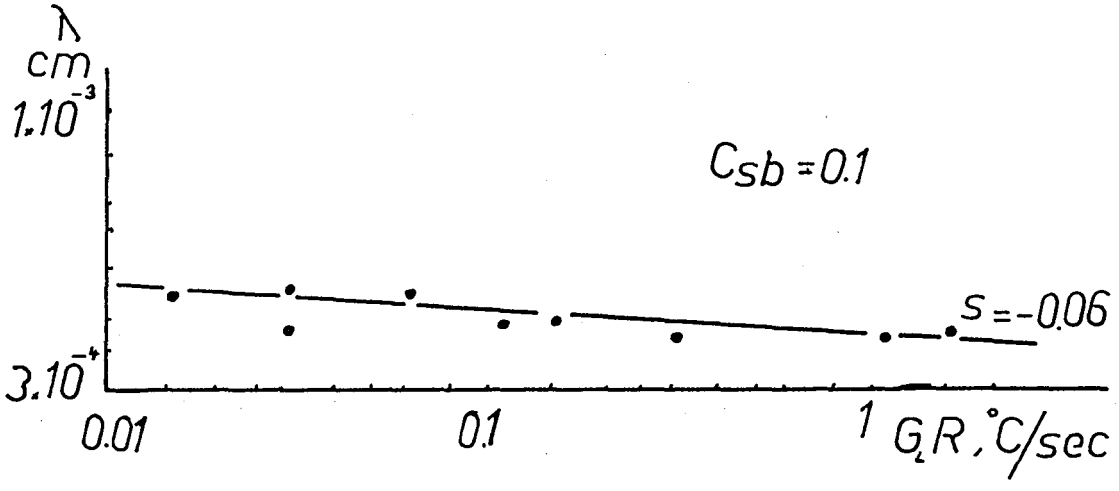

Figure 34 - Interparticle spacing versus cooling rate plot.

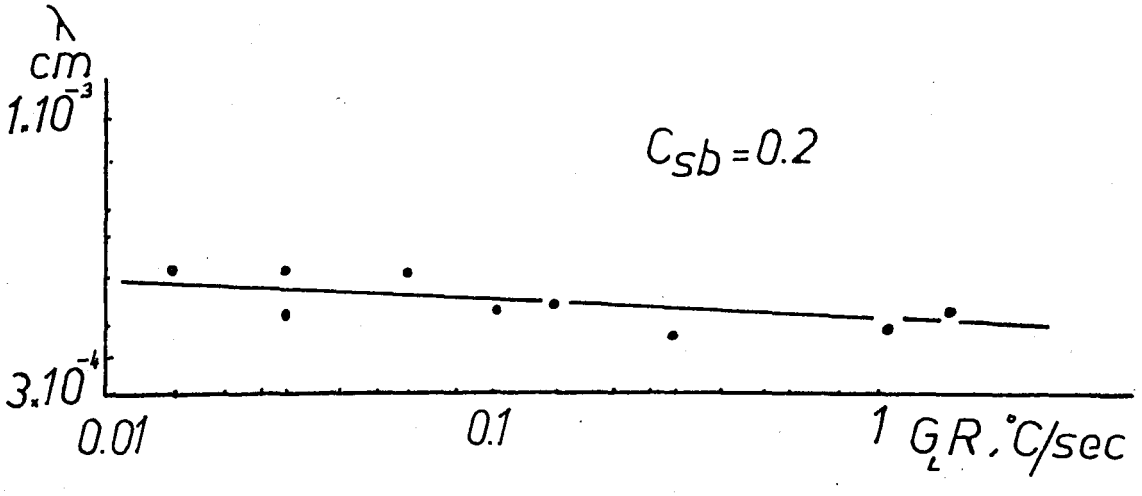

Figure 35 - Interparticle spacing versus cooling rate plot.

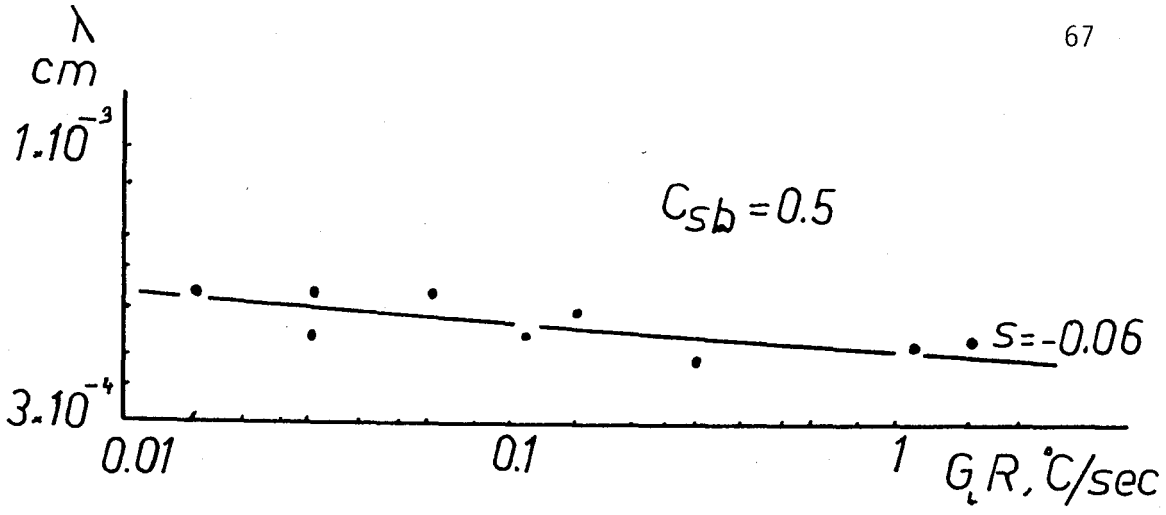

Figure 36 - Interparticle spacing versus cooling rate plot.

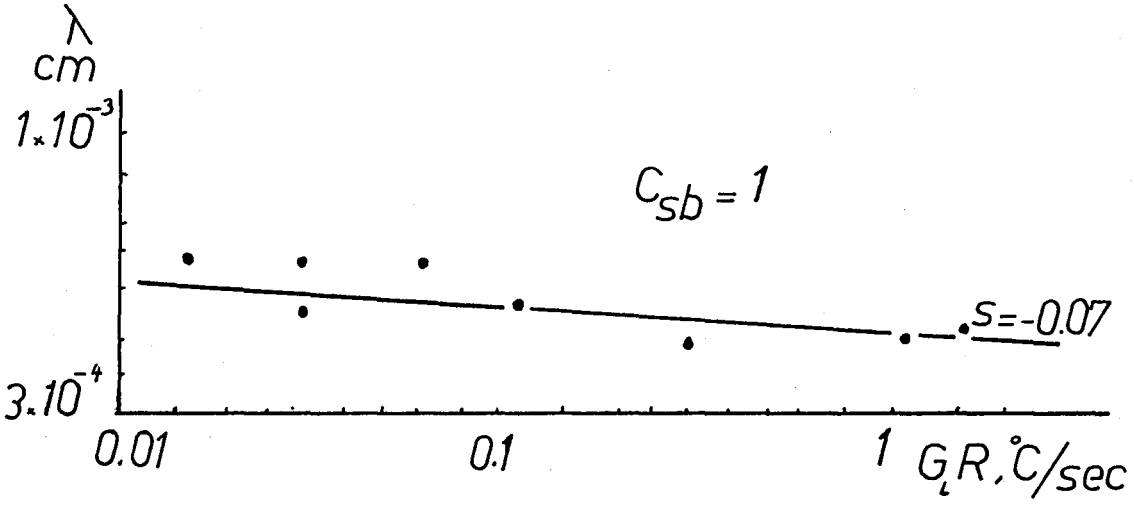

Figure 37 - Interparticle spacing versus cooling rate plot.

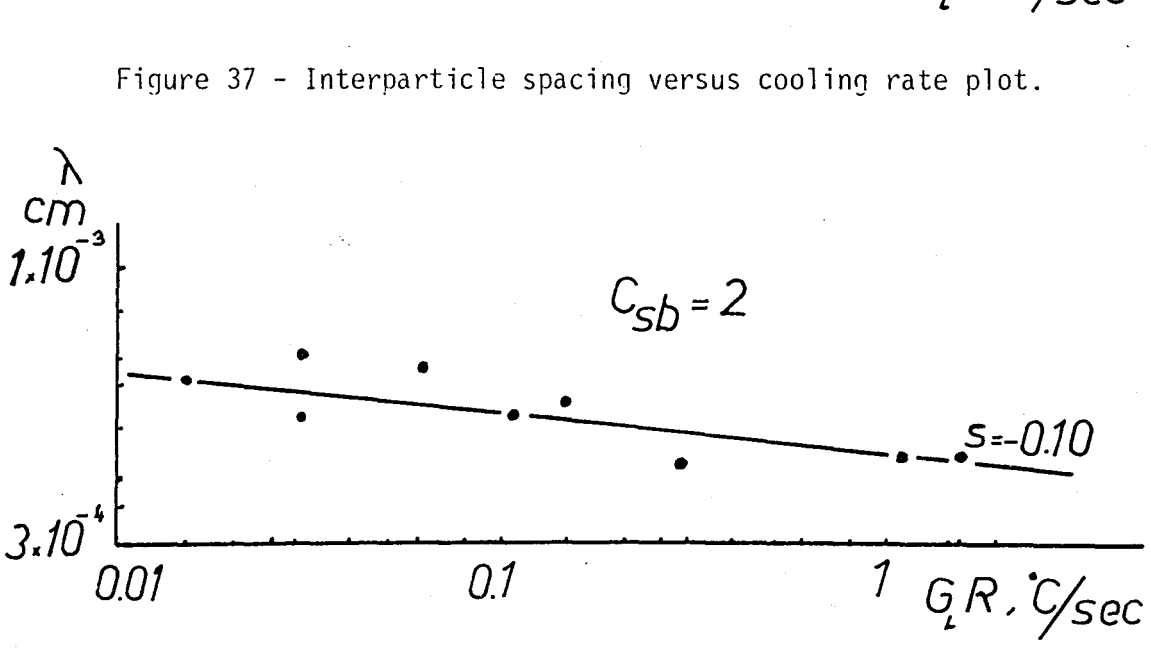

Figure 38 - Interparticle spacing versus cooling rate plot.

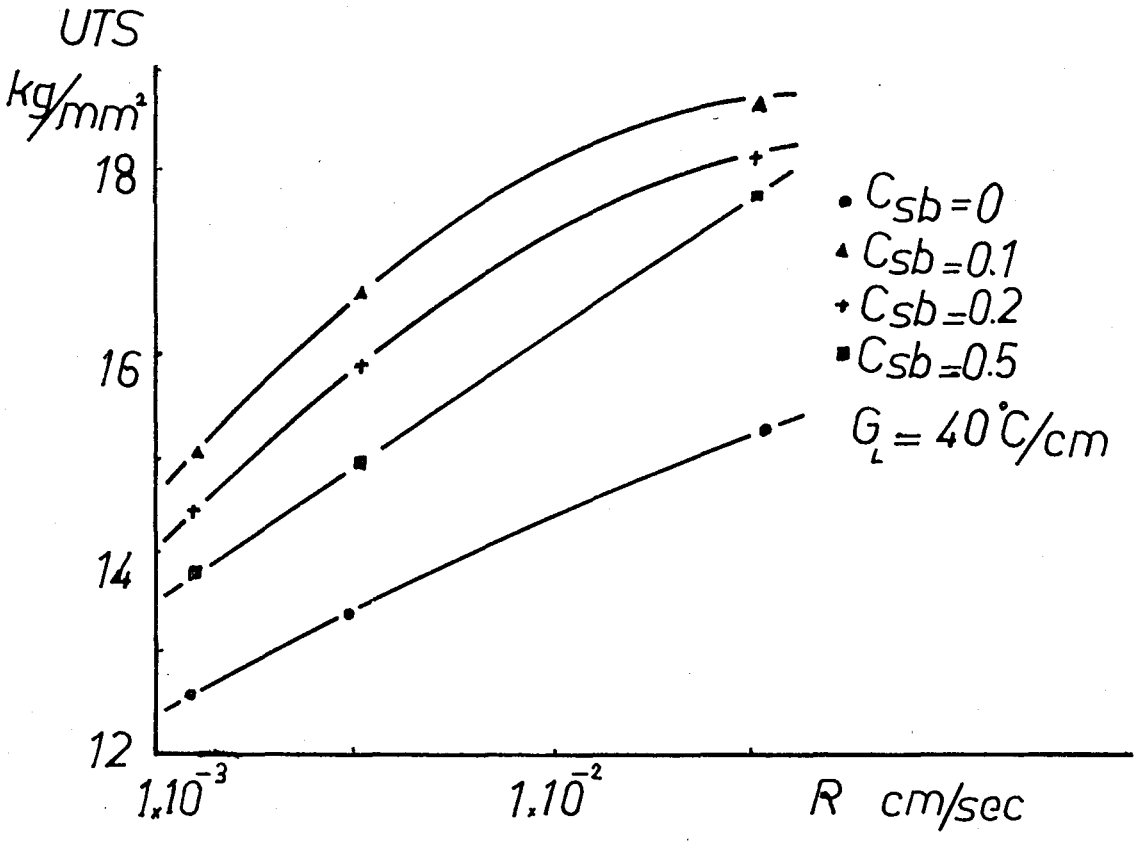

Figure 39 - Ultimate tensile strength versus growth rate plot.

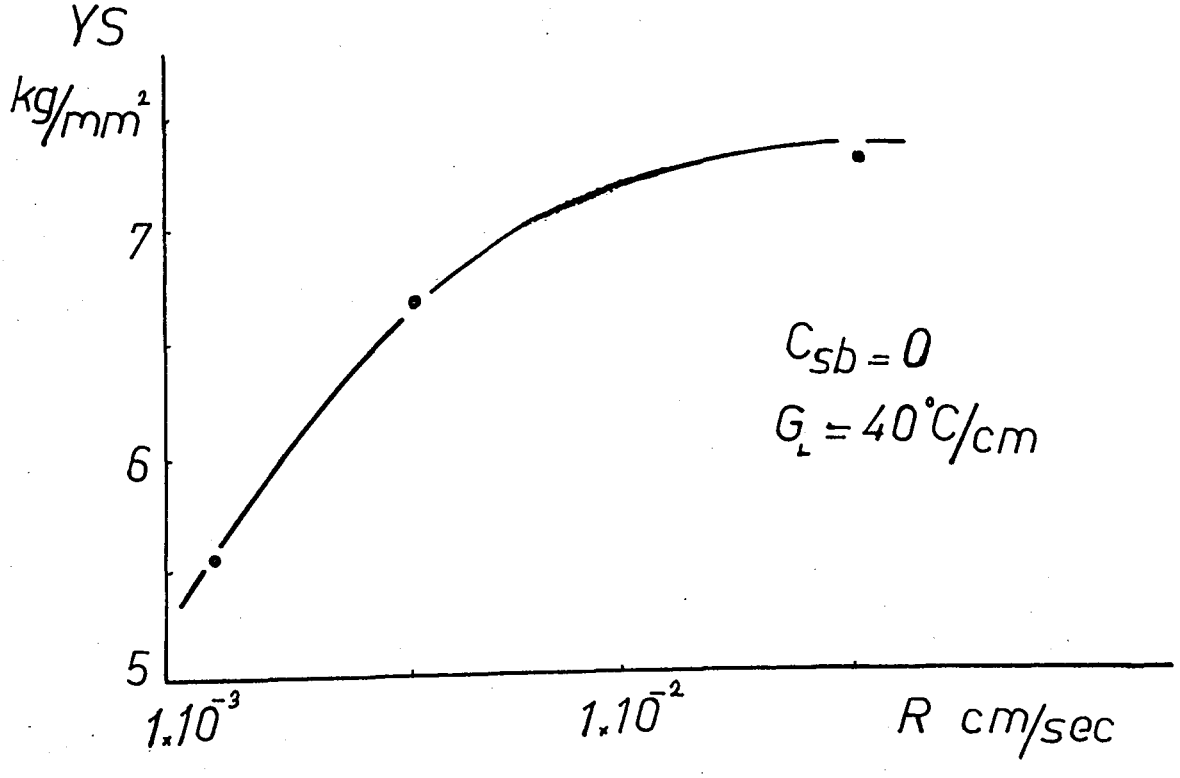

Figure 40 - Yield strength versus growth rate plot.

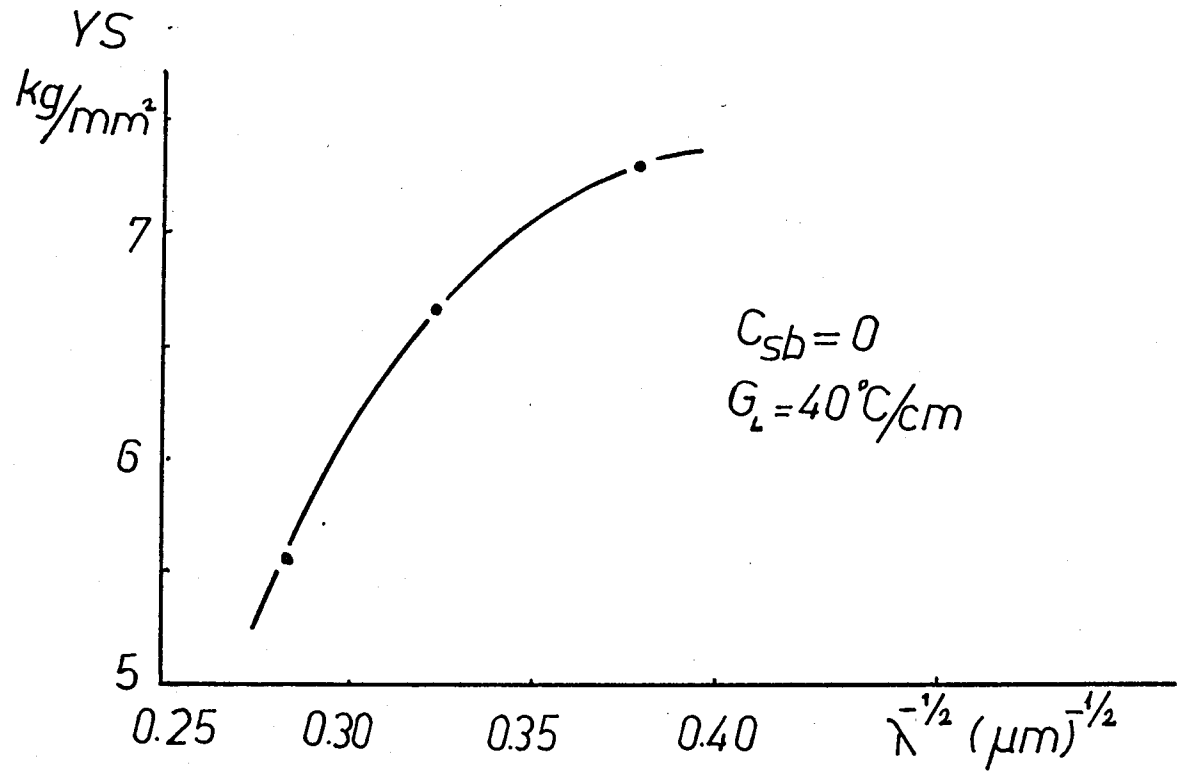

Figure 41 - Yield strength versus interparticle spacing, $\lambda^{-\frac{1}{2}}$ plot.

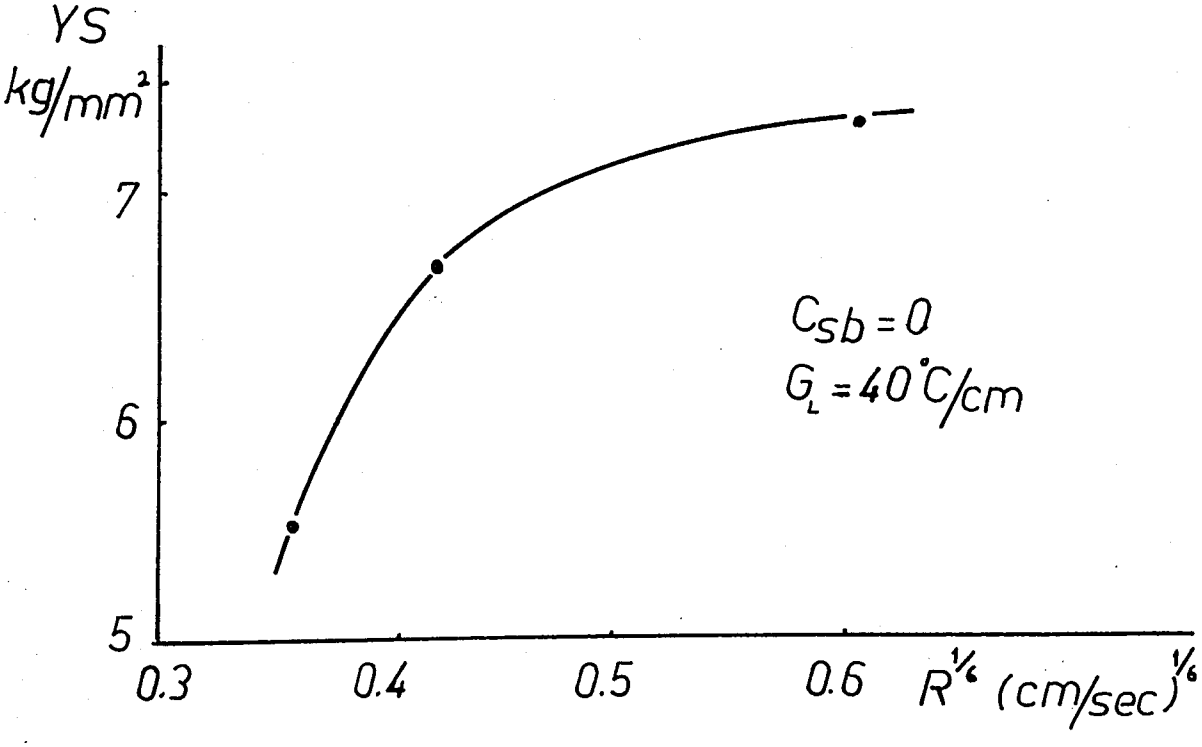

Figure 42 - Yield strength versus growth rate, $R^{1/6}$ plot.

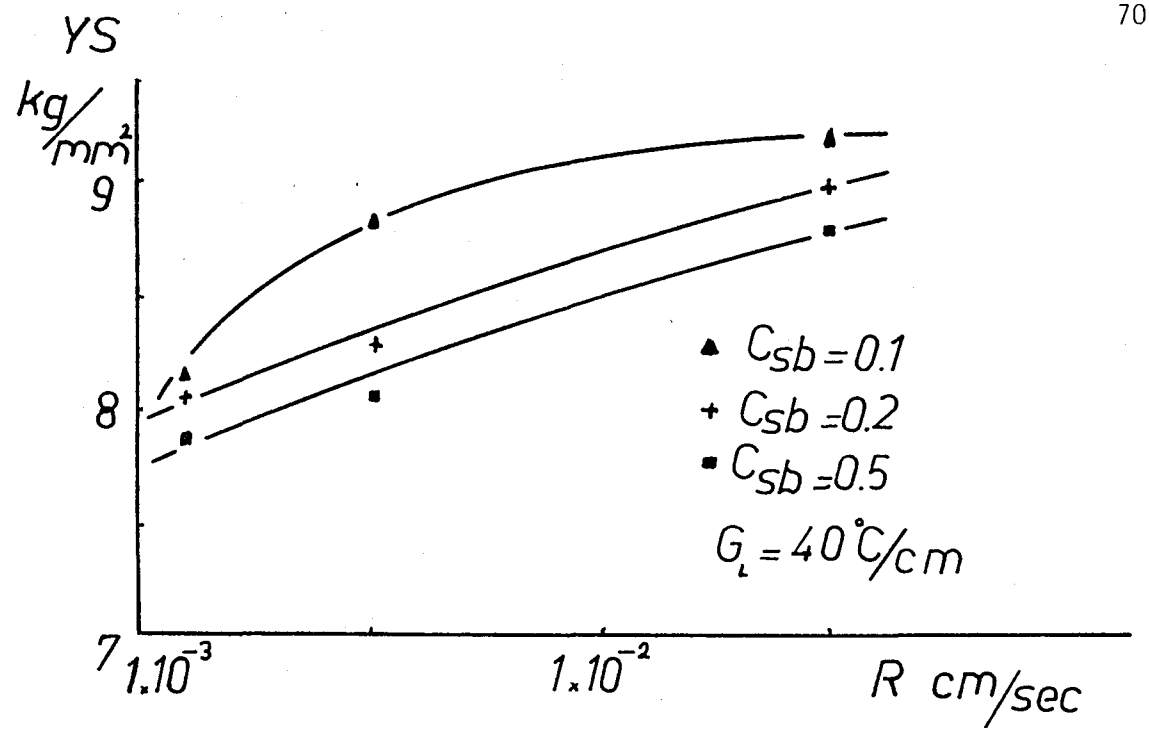

Figure 43 - Yield strength versus growth rate plot.

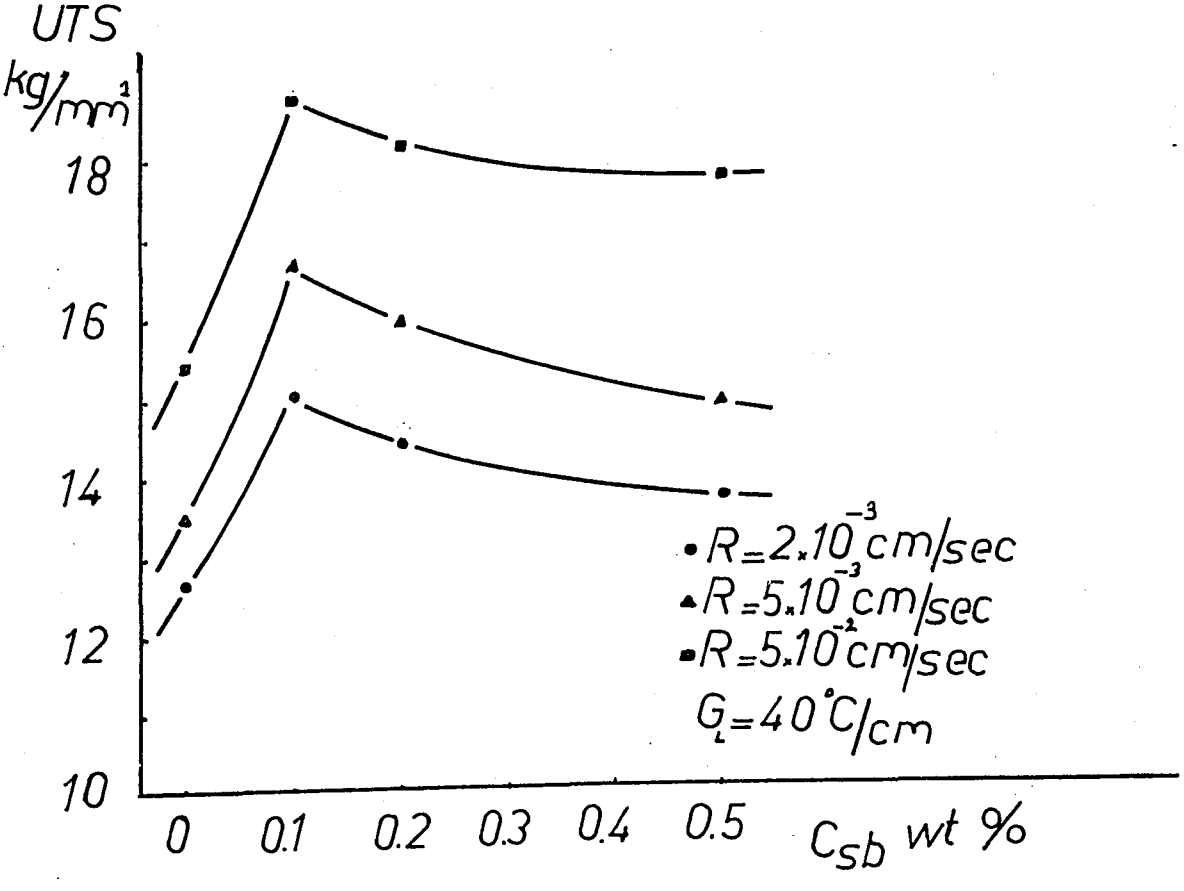

Figure 44 - Ultimate tensile strength versus antimony concentration plot.

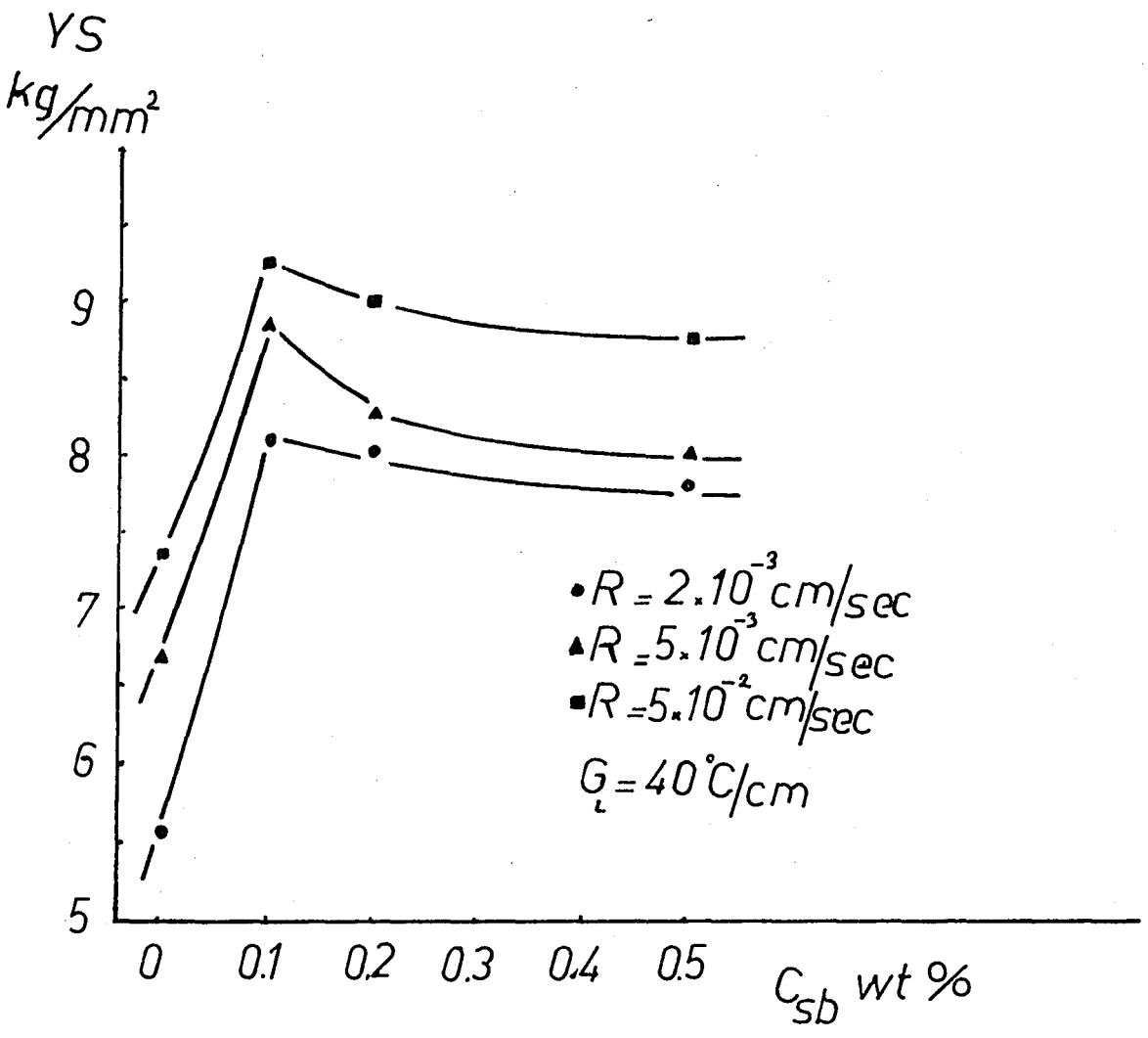

Figure 45 - Yield strength versus antimony concentration plot.

BIBLIOGRAPHY

1. Flood, S.C., and J.D. Hund, "Modification of Al-Si Eutectic Alloys with Na", The Metals Society, Vol. 15, 1981.

2. Nagel, G., and R. Portalier, "Structural Modification of Al-Si Alloys by Antimony Treatment", AFS Cast Metals Research Journal, pp. 2, December 1980.

3. Scheil, E., Z. Für Metallk., Vol. 45, pp. 298, 1954.

4. Chadwick, G.A., "Controlled Eutectic Growth", The Solidification of Metals Iron and Steel Institute, Session B, pp. 138, 1967.

5. Hunt, J.D., and K.A. Jackson, Trans. AIME, Vol. 236, pp. 1129, 1966.

6. Elliott, R., "Eutectic Solidification", International Metals Reviews, pp. 161, September 1977.

7. Jordan, R.M., and J.D. Hunt, "The Growth of Lamellar Eutectic Structures", Metallurgical Transactions, Vol. 2, pp. 3401, December 1971.

8. Chalmers, B., Principles of Solidification, New York: John Wiley, Inc., 1967.

9. Clark, J.N., Metallurgical Transactions, Vol. 6A, pp. 232, 1975.

10. Flemings, M.C., The Solidification of Castings and Ingots, New York: John Wiley, Inc., 1966.

11. Day, M.C., "Growth Forms of Eutectic Silicon and Metal-non-Metal Eutectic Systems", The Solidification of Metals Iron and Steel Institute, Session B, pp. 177, 1967.

12. Steen, H.A.H., and A. Hellawell, "Structure and Properties of Al-Si Eutectic Alloys", Acta Metallurgica, Vol. 20, pp. 363, March 1972.

13. Pacz, A., U.S. Patent 1,387,900, August 1921.

14. Smith, R.W., "Modification of Al-Si Alloys", The Solidification of Metals Iron and Steel Institute, Session B, pp. 226, 1967.

15. Steen, H.A.H., and A. Hellawell, "The Growth of Eutectic Silicon Contribution to Undercoolings", Acta Metallurgica, Vol. 23, pp. 529, 1975.

16. Fredriksson, H., J. Int. Met., Vol. 101, pp. 285, 1973.

17. Yaneva, S.B., N.V. Stoichev, and A.D. Panajotova, "Dissolution of Si in Al-Si Melts Effect of Sb on the Crystallization Process and As-Cast Structure of Al-Si Alloys", Crystal Research and Technology, pp. 737, 1981.

18. Hansen, M., and K. Anderko, "Constitution of Binary Alloys", London, 1958.

19. Yılmaz, F., Ph.D. Thesis, University of Manchester, 1979.

20. Yılmaz, F., and R. Elliott, "Structural Modification of Al-Si Alloys", Bulletin of the School of Engineering of Sakarya, pp. 84, 1981.

21. Jenkinson, D.C., and L.M. Hogan, Journal of Crystal Growth, Vol. 28, pp. 171, 1975.

22. Justi, S., and R.H. Bragg, "Tensile Properties of Directionally Solidified Al-Si Eutectic", Metallurgical Transactions, Vol. 9A, pp. 515, 1978.

23. Chadwick, G.A., "Yield Point Analysis in Eutectic Alloys", Acta Metallurgica, Vol. 24, pp. 1137, 1976.

24. Carti, C.W., P. Cotterill, and G.A. Fitzpatrick, "The Evaluation of the Interparticle Spacing in Dispersion Alloys", International Metals Review, Vol. 19, pp. 77, 1974.

25. Weinberg, F., Tools and Techniques in Physical Metallurgy, New York, 1970.

26. Winegard, W.C., Solidification of Metals, London, 1964.

APPENDIX

TABLE 2

C_{Sb} wt%	G_L $^oC/cm$	R cm/sec	A	B	C	D	E	F	G
0	40	0.002	14.71	12.5	13.40	13.16	14.16	13.16	12.72
0	25	0.002	12.94	12.5	11.90	13.65	14.43	13.65	12.10
0	10	0.002	11.73	11.54	11.54	11.90	12.30	13.40	11.73
0	40	0.005	9.38	9.40	9.26	9.15	9.50	9.50	9.04
0	25	0.005	9.26	9.25	9.04	9.15	9.50	10.00	9.15
0	10	0.005	9.26	9.01	9.04	9.26	9.47	9.50	9.38
0	40	0.05	8.62	6.94	7.81	7.98	8.06	8.33	8.06
0	25	0.05	6.81	6.35	7.01	7.90	8.53	8.43	7.98
0	10	0.05	7.35	6.25	6.52	6.58	6.41	6.36	6.52

TABLE 3

C_{Sb} wt%	G_L $^oC/cm$	R cm/sec	A	B	C	D	E	F	G
0.1	40	0.002	5.48	5.60	5.91	5.95	6.20	5.86	6.20
0.1	25	0.002	5.56	5.56	6.25	6.10	6.36	6.00	6.30
0.1	10	0.002	6.00	5.52	6.25	6.41	6.30	6.47	6.20
0.1	40	0.005	5.56	4.93	5.34	5.03	5.17	5.10	5.25
0.1	25	0.005	5.10	4.87	5.28	5.03	5.10	4.93	5.32
0.1	10	0.005	4.90	4.75	5.28	5.03	5.00	4.90	5.00
0.1	40	0.05	4.41	4.39	4.49	4.41	4.46	4.41	4.47
0.1	25	0.05	4.39	4.36	4.41	4.39	4.44	4.36	4.39
0.1	10	0.05	4.29	4.31	4.31	4.41	4.39	4.39	4.41

TABLE 4

C_{Sb} wt%	G_L $^oC/cm$	R cm/sec	A	B	C	D	E	F	G
0.2	40	0.002	6.20	6.05	6.52	6.47	6.94	6.41	6.82
0.2	25	0.002	6.20	6.15	6.47	6.47	6.88	6.47	6.70
0.2	10	0.002	6.58	6.15	6.41	6.36	6.41	6.41	6.47
0.2	40	0.005	5.64	5.32	5.46	5.56	5.56	5.46	5.56
0.2	25	0.005	5.56	5.32	5.46	5.40	5.43	5.43	5.43
0.2	10	0.005	5.56	5.21	5.73	5.21	5.52	5.21	5.56
0.2	40	0.05	5.10	5.07	5.32	5.25	5.32	5.28	5.28
0.2	25	0.05	4.97	4.81	4.84	4.93	4.90	4.90	4.90
0.2	10	0.05	4.72	4.60	4.81	4.81	4.90	4.66	4.87

TABLE 5

C_{Sb} wt%	G_L $^oC/cm$	R cm/sec	A	B	C	D	E	F	G
0.5	40	0.002	6.36	6.25	6.25	6.76	7.14	6.82	6.94
0.5	25	0.002	6.36	6.25	6.58	6.58	6.94	6.58	6.88
0.5	10	0.002	6.64	6.20	6.64	7.01	6.58	6.58	6.58
0.5	40	0.005	6.30	5.81	5.68	5.68	5.77	5.60	6.10
0.5	25	0.005	5.60	5.43	5.77	6.20	6.30	5.68	6.30
0.5	10	0.005	5.60	5.40	5.64	5.86	5.86	5.77	5.64
0.5	40	0.05	5.36	5.10	5.32	5.36	5.25	5.40	5.32
0.5	25	0.05	5.00	5.03	5.10	5.43	5.32	5.25	5.10
0.5	10	0.05	4.84	4.72	4.87	4.87	4.93	4.87	4.93

TABLE 6

C_{Sb} wt%	G_L °C/cm	R cm/sec	A	B	C	D	E	F	G
1	40	0.002	6.88	6.82	7.14	6.82	6.82	7.01	7.43
1	25	0.002	6.58	6.88	7.58	6.94	7.01	6.94	6.94
1	10	0.002	6.69	6.76	6.76	6.76	6.82	6.88	6.88
1	40	0.005	6.58	5.95	6.00	6.00	6.25	6.30	6.25
1	25	0.005	5.86	5.81	5.91	6.20	6.30	6.25	6.30
1	10	0.005	5.77	5.56	5.68	5.91	5.95	5.95	5.86
1	40	0.05	5.21	5.17	5.07	5.91	5.32	5.46	5.32
1	25	0.05	5.03	5.10	5.17	5.03	5.28	5.28	5.14
1	10	0.05	4.90	4.93	5.00	4.97	5.28	4.90	5.03

TABLE 7

C_{Sb} wt%	G_L $^oC/cm$	R cm/sec	A	B	C	D	E	F	G
2	40	0.002	7.28	7.98	8.62	7.21	7.81	7.28	7.43
2	25	0.002	7.35	8.06	7.50	8.62	7.90	7.90	8.06
2	10	0.002	7.81	7.28	7.35	7.90	8.43	8.33	8.43
2	40	0.005	6.64	6.58	6.94	7.35	7.14	7.14	6.94
2	25	0.005	7.08	6.25	7.21	6.82	6.64	6.76	6.76
2	10	0.005	6.10	6.30	6.64	6.76	6.70	6.52	6.82
2	40	0.05	5.60	5.25	5.52	5.95	5.64	5.40	5.73
2	25	0.05	5.60	5.17	5.25	5.77	5.32	5.81	5.43
2	10	0.05	5.25	5.00	5.10	5.46	5.43	5.32	5.32

TABLE 8

C_{Sb} wt%	G_L $^oC/cm$	R cm/sec	A	B	C
0	25	0.002	13.16	12.50	11.72
0.1	25	0.002	5.60	5.60	6.10
0.2	25	0.002	6.25	6.15	6.52
0.5	25	0.002	6.36	6.25	6.64
1	25	0.002	6.69	6.88	7.66
2	25	0.002	7.42	7.89	7.57

TABLE 9

G_L	C_{Sb}	Growth rate	Ult.Tensile Strength	0.2 Pct offset yield strength	Vickers Hardness Number	Elongatio
$^oC/cm$	wt%	cm/sec	kg/mm^2	kg/mm^2	kg/mm^2	%
40	0	0.002	12.64	5.57	55.15	3.5
40	0.1	0.002	15.09	8.11	63.19	6.0
40	0.2	0.002	14.46	8.09	61.26	5.0
40	0.5	0.002	13.84	7.87	60.33	3.8
40	0	0.005	13.52	6.72	58.23	3.8
40	0.1	0.005	16.73	8.90	72.33	9.0
40	0.2	0.005	16.04	8.30	63.53	7.8
40	0.5	0.005	15.03	8.07	62.54	5.5
40	0	0.05	15.47	7.36	68.08	3.7
40	0.1	0.05	18.86	9.30	80.19	7.5
40	0.2	0.05	18.24	8.93	74.39	7.3
40	0.5	0.05	17.92	8.86	70.35	6.5
10	0	0.002	12.73	5.65	55.96	3.5
10	0.1	0.002	15.09	8.04	63.53	5.8
10	0.2	0.002	14.42	7.92	61.89	5.0
10	0.5	0.002	13.95	7.85	60.33	4.0
10	0	0.05	15.59	7.42	68.83	3.8
10	0.1	0.05	18.74	9.26	77.43	7.3
10	0.2	0.05	18.23	9.00	74.82	7.0
10	0.5	0.05	18.10	8.92	72.33	6.5